Original Paper

K. Bales, S. Dewji, E. Sanchez

Comparison of neutron organ and effective dose coefficients for PIMAL stylized phantom in bent postures in standard irradiation geometries

K. Bales, S. Dewji (✉), E. Sanchez
Oak Ridge National Laboratory, Center for Radiation Protection Knowledge, Oak Ridge, TN, USA
E-mail: dewjisa@ornl.gov

K. Bales
University of Tennessee – Knoxville, Department of Nuclear Engineering, Knoxville, TN, USA

E. Sanchez
Massachusetts Institute of Technology, Department of Nuclear Science and Engineering, Cambridge, MA, USA

Notice: This manuscript has been authored by UT-Battelle, LLC, under Contract No. DE-AC0500OR22725 with the U.S. Department of Energy. The United States Government retains and the publisher, by accepting the article for publication, acknowledges that the United States Government retains a non-exclusive, paid-up, irrevocable, world-wide license to publish or reproduce the published form of this manuscript, or allow others to do so, for the United States Government purposes. The Department of Energy will provide public access to these results of federally sponsored research in accordance with the DOE Public Access Plan (http://energy.gov/downloads/doe-public-access-plan).

Abstract Neutron dose coefficients for standard irradiation geometries have been reported in International Commission on Radiological Protection (ICRP) Publication 116 for the ICRP Publication 110 adult reference phantoms. In the present work, organ and effective dose coefficients have been calculated for a receptor in both upright and articulated (bent) postures representing more realistic working postures exposed to a mono-energetic neutron radiation field. This work builds upon prior work by Dewji and co-workers comparing upright and bent postures for exposure to mono-energetic photon fields. Simulations were conducted using the Oak Ridge National Laboratory's articulated stylized adult phantom, "Phantom wIth Moving Arms and Legs" (PIMAL) software package, and the Monte Carlo N-Particle (MCNP) version 6.1.1 radiation transport code. Organ doses were compared for the upright and bent (45° and 90°) phantom postures for neutron energies ranging from $1 \cdot 10^{-9}$ to 20 MeV and the ICRP Publication 116 external exposure geometries – antero-posterior (AP), postero-anterior (PA), and left and right lateral (LLAT, RLAT). Using both male and female phantoms, effective dose coefficients were computed using ICRP Publication 103 methodology. The resulting coefficients for articulated phantoms were compared to those of the upright phantom. Computed organ and effective dose coefficients are discussed as a function of neutron energy, phantom posture, and source irradiation geometry. For example, it is shown here that for the AP and PA irradiation geometries, the differences in the organ coefficients between the upright and bent posture become more pronounced with increasing bending angle. In the AP geometry, the brain dose coefficients are expectedly higher in the bent postures than in the upright posture, while all other organs have lower dose coefficients, with the thyroid showing the greatest difference. Overall, the effective dose estimated for the upright phantom is more conservative than that for the articulated phantom, which may have ramifications in the estimation or reconstruction of radiation doses.

Introduction

Estimation of radiation dose in the human body is a complex problem necessitating the use of computational modeling of the exposure geometry and mathematical representation of the human body by means of anthropomorphic phantoms. Using the methodology in the International Commission on Radiological Protection (ICRP) Publication 103 (ICRP 2007), the equivalent dose coefficients calculated in organs and tissues of the reference male and female phantoms are used to determine the effective dose. A revision of the dose coefficients found in ICRP Publication 74 (ICRP 1996) has been released in ICRP Publication 116, employing the ICRP Publication 110 reference adult phantoms (ICRP 2009) for the standard irradiation source geometries: antero-posterior (AP), postero-anterior (PA), left and right lateral (LLAT, RLAT), and isotropic (ISO) radiation fields. While ICRP Publication 116 tabulates dose coefficients for the exposure source geometries employed in the present work, those ICRP coefficients were determined using computational phantoms positioned in an upright position derived from computed tomography (CT) scans in the supine position, published as the ICRP reference adult male and female phantoms in ICRP Publication 110 (ICRP 2009).

Most dose reconstruction studies have been performed using an upright phantom, which may not provide a good dose estimate for the body postures likely to be encountered in an occupational setting. In addition, real-world exposures do not involve parallel mono-energetic beams or isotropic fields; therefore, this work focuses on the effect of body posture. Some works have already argued that posture is critical for dose reconstruction involving a seated subject (Dewji et al. 2014, Han et al. 2014, Alves et al. 2016). There are only few studies in which phantoms in a specific working posture have been explored for dose reconstruction purposes and fewer have been explored with a focus on the neutron source variable. Akkurt et al (2009) investigated dose received by a glovebox worker in a realistic posture using a phantom with extended arms (Akkurt and Eckerman 2007) for both a neutron spectrum, as well as a clean weapons-grade plutonium source. Additionally, Vasquez et al. (2014) recreated postures observed from a motion capture system to more accurately assess doses received by two workers in the criticality accident that took place in Tokai-Mura, Japan in 1999.

In the work explored here, dose calculations were performed using upright and bent phantom postures to analyze the differences in dose due to these various postures in standard irradiation mono-energetic neutron fields. This work builds upon prior work by

Dewji et al. (2017), which represents the photon counterpart of the work conducted here. Both these works explore the role of body posture in dose reconstruction for four of the irradiation geometries of ICRP Publication 116 (2010).

Methods

PIMAL phantom

Mathematical models of the human body models have almost exclusively been created in a rigid, upright posture (Xu 2014). The "**P**hantom w**I**th **M**oving **A**rms and **L**egs" (PIMAL) software developed by Oak Ridge National Laboratory employs a graphical user interface (GUI) to allow for a customizable geometry of the phantom (Akkurt and Eckerman 2007). Phantom geometry can be described using slider bars or a textbox to input joint angle for the shoulder, elbow, knee and hip joints. The GUI, captured in prior work by Dewji et al. (2017), allows the user to visualize and adjust the position of the arms and legs. PIMAL has been updated to include two separate reference stylized male and female phantoms (Dewji and Hiller, 2016) with tissue compositions and densities from ICRP Publication 89 (ICRP 2002), and to include the ICRP 110 reference voxel phantoms (ICRP 2009); however, these phantoms remain in a static upright position. Prior work by Bellamy et al. (2016) and Hiller and Dewji (2017) compare, in detail, the anatomical differences between reference adult voxel and stylized phantom in an external air submersion cloud of mono-energetic photons for the updated ORNL stylized phantoms. In these studies, the voxel resolution of thin-walled organs, intra-organ position, and elaboration of skeletal response functions for bone surface and active marrow dosimetry contributed the greatest variation in organ and effective dose coefficients for external photon irradiation sources. The differences between the upright voxel and stylized phantoms are detailed in these studies, and the reader is referred to these works for comparisons and subsequent justification for comparable organ dose values for voxel and stylized phantoms due to external radiation sources.

After the phantom has been positioned to the user's specifications and the parameters have been set, PIMAL creates and executes an input file for the Monte Carlo N-Particle (MCNP) radiation transport code. Organ dose coefficients may then be extracted from the MCNP output files. The simulation part of PIMAL allows the user to set various parameters for the simulation: the mode specifies neutron and/or photon sources, the source energy allows the user to set external and internal sources for mono-energetic neutron/photon energy, external source geometries allow the user to select a point source with user-specified X, Y, Z coordinates, or source geometries listed in ICRP Publication 116, internal source geometries allow organ volume sources to be set in the body, and the MCNP Input Generation and Execution allows the code to be run within PIMAL, producing an organ dose table that can be exported as an ASCII file. The MCNP output file is also saved and can be used to analyze the derived dose coefficients in detail.

In the present work, the organ and effective dose coefficients for the bent posture are compared to those for an upright posture, and the coefficients for the upright posture were compared to those tabulated in ICRP Publication 116. PIMAL was used to orient the torso of male and female phantoms with repositioned arms and legs at 45° and 90° from the vertical axis (half and full bent postures) to represent the effects of articulated postures in theoretical exposure fields (Fig. 1).

Fig 1 The upright, half-bent (45º), and full-bent (90º) side views taken from the PIMAL 4.1.0 GUI for the stylized phantom.

Monte Carlo simulations

The 6.1.1 version of the MCNP radiation transport code (Pelowitz at al. 2014) was used to calculate the absorbed doses in each of the organs. Using both male and female stylized phantoms represented in PIMAL, organ dose data was computed using MCNP for each of the five irradiation geometries using upright, half-bent (45°), and full-bent phantoms (90°). These simulations were conducted for the following range of mono-energetic neutron energies for each case: $1 \cdot 10^{-9}$ to 20 MeV. A 200 cm $\times$ 200 cm plane was used for each irradiation geometry, placed 1 m from the center of the PIMAL phantom. The simulations were run in a vacuum.

Organ doses were computed using the MCNP +F6 collision heating tally in MeV/g. Doses for active marrow and bone surface were estimated by applying the skeletal response functions of ICRP Publication 116 (ICRP 2010) to the MCNP F4 tally in particles/cm^2 in the skeletal regions outside of PIMAL. All simulations were run until statistical errors converged within < 10% for most neutron energies.

Effective dose calculations

Using the organ dose coefficients provided from the MCNP simulations, the effective dose coefficient, E, was calculated using the methodology of ICRP Publication 103 (2007). Effective dose coefficient was determined as follows:

$$E = \sum_T w_T \left[\frac{H_T^M + H_T^F}{2}\right] \tag{1}$$

where H_T^M is the equivalent dose coefficient in organ/tissue T for the male phantom, H_T^F is the equivalent dose coefficient in organ/tissue T for the female phantom, and w_T is the tissue weighting factor for organ/tissue T. The tissue weighting factors defined in ICRP Publication 103 are shown in Table 1.

Table 1 ICRP Publication 103 tissue weighting factors (International Commission on Radiological Protection 2007).

Tissue	w_T	$\sum w_T$
Bone-marrow (red), Colon, Lung, Stomach, Breast, Remainder tissues*	0.12	0.72
Gonads	0.08	0.08
Bladder, Esophagus, Liver, Thyroid	0.04	0.16
Bone surface, Brain, Salivary glands, Skin	0.01	0.04
Total		1.00

*Remainder tissues: Adrenals, Extrathoracic region, Gall bladder, Heart, Kidneys, Lymphatic nodes, Muscle, Oral mucosa, Pancreas, Prostate (M), Small intestine, Spleen, Thymus, Uterus/cervix (F)

Male and female equivalent dose coefficients are computed as:

$$H_T = \sum_R w_R D_{T,R} \tag{2}$$

where w_R is the radiation weighting factor and $D_{T,R}$ is the absorbed dose from radiation *R* to organ/tissue *T*. For this work, the radiation weighting factors for neutrons from ICRP Publication 103 (2007) are employed:

$$w_R = \begin{cases} 2.5 + 18.2e^{-[ln(E_n)]^2/6}, & E_n < 1\text{ MeV} \\ 5.0 + 17.0e^{-[ln(2E_n)]^2/6}, & 1\text{ MeV} \le E_n \le 50\text{ MeV} \\ 2.5 + 3.25e^{-[ln(0.04E_n)]^2/6}, & E_n > 50\text{MeV} \end{cases} \tag{3}$$

where w_R is a function of neutron energy, E_n.

Since neutrons are uncharged, energy is imparted through collisions and absorption with nuclides to tissues by secondary particles; i.e., liberated charged particles and photons. Element composition and density of the tissues can have an impact on the imparted energy. The photon dose contribution is strongly dependent on neutron energy. For example, at low energies (e.g. thermal energy), the contribution of neutron-liberated photons dominates the absorbed dose. The radiation weighting factors, found in ICRP Publication 103 (2007) and shown in Fig. 2 reflect the relative energy deposition via neutron interactions. Equivalent dose coefficients were computed using Eq. 2 and employing the radiation weighting factors found in Eq. 3. The MCNP F4 tally used to determine dose rates for the active marrow and endosteum separated the neutron and photon contributions, while the dose rates determined for the other organs and tissues did not. The two were added together to determine the total dose for each irradiation geometry, energy, and posture. The energy-dependent neutron weighting factors were then applied to the total dose from the neutrons and secondary particles for the skeletal organs.

Results and discussion

Organ absorbed dose ratios

The sex-averaged organ absorbed dose coefficients for the bent postures were compared to the upright posture. These calculated ratios are found in Table 2 for the 45º bent posture and in Table 3 for the 90º bent posture for each of the irradiation geometries. Organ dose coefficients that showed strong posture variation are depicted in Figs. 3-11[1].

When analyzing ratios of the organ absorbed dose coefficients, it is important to note that a ratio greater than one (ratio >1) means that the coefficient derived for the upright posture is less than that based on the bent posture. If the ratio is less than one, then the

[1] Supplemental electronic data has been provided in Tables 5-40 and Figures 16-25 for sex-specific organ dose coefficients for all organs and neutron energies for AP, PA, LLAT, and RLAT irradiation geometries.

opposite holds where the dose for the upright posture is greater than the bent posture. The ratios calculated for the AP irradiation geometry show significant differences between the bent and upright postures, and these differences become more pronounced with increasing bending angle. The brain receives higher doses in the bent postures than the upright; it receives as much as 65% for the 45º posture at $1 \cdot 10^{-9}$ MeV and 90% more dose for the 90º posture at the 1 MeV neutron energy (Fig 3). There is no distance-dependence for a parallel beam source in a vacuum; therefore, the fact that the ratio is greatest at the lower neutron energies suggests that the photon contribution is higher in the bent geometry. While the brain dose is greater in the bent than in the upright phantom, all other organs receive a smaller dose for the AP geometry. Most notably, the thyroid shows the lowest ratio (a lower dose received) (Table 3). The thyroid receives 77% less dose in the half-bent posture and 94% for the full bent posture at the 1 MeV neutron energy (Table 2). The ratio decreases as a function of energy from $1 \cdot 10^{-9}$ to 1 MeV and increases as a function of energy from 1 to 20 MeV, meaning that the dose to the phantom in the 45º posture (Table 2) approaches the dose to the upright phantom[2]. For the 90º posture, the doses to the abdominal organs (liver, bladder, small intestine, pancreas, kidneys, gall bladder, adrenals, stomach) are much higher for the upright phantom than for the bent, and the thoracic organs (extrathoracic region, lungs, breast) are better represented by the upright phantom than other organs (Table 3).

For the PA irradiation geometry, the urinary bladder, testes, and prostate become more susceptible to increased exposure in a bent posture, where the absorbed doses to all other organs were less than in the upright phantom (Fig 4, Fig 9-10). Clearly, absorbed organ dose is dependent on posture; the testes and prostate receive more dose in the full-bent posture, as these organs are more exposed to the radiation source in the male phantom with increasing bending angle. The doses to the urinary bladder are slightly lower in the half-bent posture than in the upright for the $1 \cdot 10^{-9}$ to 0.5 MeV energy range and very slightly larger for energies 0.7 to 20 MeV. The dose to the urinary bladder is lower than in the upright posture by as much as 42% at 0.1 MeV, but only slightly lower for energies

[2] See supplemental electronic data: Tables 27-28 for organ absorbed dose for thyroid and Figure 16 for ratio plot.

ranging from 2 MeV to 20 MeV in the full-bent posture. The testes show ratios greater than 1 when compared to the upright male phantom by factors of 2.27 and 4.01 in the 45º and 90º postures, respectively, at 1 MeV. The prostate receives doses that are higher than those to upright male posture by a factor of 3.03 in the half-bent posture at 1 MeV and a factor of 2.02 in the full-bent posture at 1.2 MeV. The dose ratios in Table 2 and Table 3 do not reflect the numbers mentioned above because the tables use sex-averaged doses, rather than sex-specific doses. Fig 9 and 10 depict the gonad and sex-specific organ doses, respectively. In the 90º posture, the doses become more pronounced for the gonads, urinary bladder, bone surface, and uterus/prostate.

For both of the lateral geometries (LLAT and RLAT), the organs located in the torso of the phantom receive more dose than they would have in the upright posture, due to the lateral geometries having the arms angled out from the body. However, there is minimal difference in organ doses between the two bent postures, as summarized in Tables 2 and 3. For the sex-averaged dose ratios, both the breast and thymus receive lower doses in the full-bent posture than the upright posture for energies 0.05 to 20 MeV, while all other organs receive doses equal to or greater than the doses to the upright phantom. For the male phantom, the testes receive lower doses when bent compared to upright for energies 0.2 to 20 MeV for both of the lateral geometries: as much as 48% lower for the half-bent posture at 1 MeV (Table 2) and 62% lower for the full bent posture at 1.2 MeV for both LLAT and RLAT (Table 3) [3]. For both LLAT and RLAT, the ratios are greater than 1 for the doses for the testes and thymus for lower energies, and the colon, lungs, stomach, urinary bladder, liver, esophagus, skin, adrenals, small intestine, kidneys, muscle, uterus/prostate, gall bladder, and heart for all energies, with the exception of the skin at 20 MeV. For the LLAT geometry, the doses to the spleen and pancreas in the bent postures are greater than in the upright phantom by factors up to three. The doses to these organs are greater than the doses for the RLAT geometry because the pancreas and spleen are located on the left side of the body. The doses differ from those to the upright phantom so drastically due to the extended arms in the bent postures, as stated above. Similarly, the liver (Fig 8) receives a higher dose in the RLAT geometry than the LLAT because it is located in the right side of the body.

[3] See supplemental electronic data: Table 11 for organ absorbed dose for testes and Figure 24 for ratio plot.

Overall, there is little variation between the two bent postures because the organs observe the same neutron fluence from the source.

Dose to the eye

The dose to the eye does not contribute to the effective dose as defined in ICRP Publication 103. However, the dose to the lens of the eye is an important consideration among medical and other radiation workers (e.g., Barnard et al. 2016). The dose depends very strongly on phantom posture in both AP and PA geometries and is generally lower in the bent phantoms than in the upright and trends towards the dose to the upright phantom with increasing energy, with the exception of the full-bent phantom in the PA geometry (Fig 11). There is little variation in the dose to the eye at either LLAT or RLAT irradiation geometries for all postures; the doses are very near those of the upright phantom.

Contribution of secondary particles

For both the active marrow and endosteum doses, photons contribute significantly to the organ absorbed dose and effective dose coefficients, even more so than the neutrons, for energies $1 \cdot 10^{-9}$ to 0.1 MeV for all irradiation geometries. From approximately 0.5 to 20 MeV, the neutrons dominate the dose coefficients. This is true for all phantom postures. These trends correlate with the plot of the neutron weighting factors, as neutrons have a larger impact in the mid-energy range and a smaller impact for low and high energies, where photons increasingly contribute. The neutron and photon contributions to the absorbed organ dose coefficients for the upright and bent postures can be seen in Fig 12 for the active marrow and Fig 13 for the endosteum for the AP irradiation geometry.

Effective dose coefficient

The effective dose coefficient was calculated with Eqs. 1 and 2 using gender-averaged organ equivalent dose coefficients and tissue and radiation weighting factors of ICRP Publication 103. The effective dose coefficient was expressed as pSv-cm^2 for each of the five irradiation geometries for each posture (upright, half bent, and full bent), and can be found in Table 4.

The most recognizable difference in effective dose coefficients between the upright and bent postures can be found in the full-bent phantom for the AP geometry, with the largest discrepancy measuring at 82% lower than that in the upright phantom, at 10 – 50 keV. The phantom in the 90º posture shows effective dose ratios (compared to upright) of less than 1 for all energies in the AP geometry (Fig 14). The coefficients for the half-bent phantom are comparable to the upright phantom for energies above 2 MeV. However, the coefficients are lower than in the upright phantom by as much as 43% for energies 2 MeV or less.

The results for the effective dose coefficients for the PA irradiation geometry behave similarly to those of the AP geometry (Fig 14). The relative difference to the upright phantom peaks at 82% for the full-bent phantom, and the 45º bent phantom shows lower effective dose coefficients when compared to the upright phantom, more so than for the AP source geometry, over all energies, peaking at 52% lower than the upright phantom.

Contrary to the results for the AP and PA irradiation geometries, the LLAT and RLAT effective dose coefficient ratios tend to have a position-independent impact, but still vary as a function of source neutron energy (Fig 15). The relative difference to the upright phantom ranges from 44% to 15% for the half-bent phantom and 46% to 15% for the full-bent posture for the LLAT geometry and from 40% to 0% for the both the bent phantom postures for the RLAT source geometry.

PIMAL upright phantom, whose values are found in Table 4, represent the effective dose values from ICRP Publication 116 well for the AP and PA irradiation geometries (ICRP 2010). The value for the effective dose in the AP geometry at $1 \cdot 10^{-5}$ MeV is 0.32% greater than that in the ICRP document, and the greatest difference occurs at 20 MeV, which is 29% less than the dose published by the ICRP. For the PA geometry, the effective dose from this work is 1.74% and 46.74% greater than the ICRP's value at 4 MeV and 0.2 MeV, respectively. The LLAT geometry shows relative differences ranging from 0.58%

greater at 0.07 MeV to 37.18% less at 20 MeV. The RLAT geometry values range from 0.81% greater at 0.005 MeV to 37.90% less at 20 MeV.[4]

Conclusion

Organ and effective dose coefficients were simulated for phantoms in half- and full-bent articulated positions and compared to the traditional upright phantom. Monoenergetic neutron irradiation fields were simulated for AP, PA, LLAT, and RLAT source geometries for energies ranging from $1 \cdot 10^{-9}$ MeV to 20 MeV. Because the effective dose coefficients for the articulated phantoms were lower than those of the upright phantom for all energies for both the AP and PA geometries, using the upright phantom would provide a conservative approach to determining effective dose. This may result in a higher-than-actual assigned dose to the receptor, which may be impactful in certain dose estimation or dose reconstruction scenarios. Both the organ absorbed dose and effective dose coefficients for the articulated phantoms were generally higher than the coefficients for the upright phantom in the LLAT and RLAT source geometries for both bent phantom postures.

Effective dose is a robust quantity, but consideration must be given to organs at risk for a receptor in an articulated position. The absorbed dose coefficients of the brain for the AP irradiation source geometry and the testes and prostate for the PA irradiation source geometry for both bent phantom postures are significantly higher than those of the upright phantom. This warrants that the posture of the receptor, as well as the location and energies of source radiation fields and source geometries, must be considered when calculating absorbed dose, in order to obtain an accurate understanding of the dose received by the organs. It is important to take realistic working postures into consideration to determine accurate results when performing dose estimations, especially noting where organ doses

[4] An expanded library of graphs of the ratios comparing the postures to the upright PIMAL phantom has been provided as electronic supplemental material as Figs 16-25 for each sex-averaged organs and the AP, PA, LLAT, and RLAT sources.

for receptors in articulated positions may be under- or over-estimated in the absence of employing an articulated phantom for dose estimation.

Acknowledgements The authors would like to thank Dr. Keith Eckerman and Dr. Ken Veinot for their invaluable feedback on this work. This work was supported in part by the U.S. Department of Energy, Office of Science, Office of Workforce Development for Teachers and Scientists (WDTS) under the Science Undergraduate Laboratory Internship program and by the United States Nuclear Regulatory Commission under Contract No. NRCHQ6017D0003.

References

Akkurt H, Eckerman KF. (2007) Development of PIMAL: Mathematical Phantom with Moving Arms and Legs, ORNL/TM-2007/14. Oak Ridge National Laboratory, Oak Ridge

Akkurt H, Bekar K, Eckerman KF (2009) Assessment of Organ Doses for a Glovebox Worker Using Realistic Postures with PIMAL and VOXMAT. Trans Am Nuc Soc 101:671-3

Alves M, Santos W, Lee C, Bolch W, Hunt J, Júnior AC (2016) Conversion coefficients for proton beams using standing and sitting male hybrid computational phantom calculated in idealized irradiation geometries. Radiat Prot Dosim 175(1), 75-86

Barnard SG, Ainsbury EA, Quinlan RA, Bouffler SD (2016) Radiation protection of the eye lens in medical workers—basis and impact of the ICRP recommendations. Brit J Radiol 89(1060), 20151034

Bellamy MB, Hiller MM, Dewji SA, Veinot KG, Leggett RW, Eckerman KF, Easterly C, Hertel NE (2016) Comparison of monoenergetic photon organ dose rate coefficients for stylized and voxel phantoms submerged in air. Radiat Prot Dosim 172(4), 367-374

Dewji SA, Bellamy MB, Hertel NE, Leggett RW, Sherbini S, Saba MS, Eckerman KF (2015) Estimated dose rates to members of the public from external exposure to patients with 131I thyroid treatment. Med Phys 42(4), 1851-1857

Dewji SA, Hiller MM (2016) PIMAL: Phantom wIth Moving Arms and Legs Version 4.1.0. US Nuclear Regulatory Commission, Rockville, NUREG/CR-7131

Dewji SA, Reed KL, Hiller MM (2017) Comparison of Organ Doses for PIMAL Stylized Phantoms in Upright and Bent Positions for Standard Irradiation Geometries. Radiat Environ Biophys56(3):277-91

Han EY, Ha W.-H., Jin Y-W, Bolch WE, Lee C (2014) Effective dose conversion coefficients for health care provider exposed to pediatric and adult victims in radiological dispersal device incident. J Radiol Prot 35(1): 37-45

Hiller M, Dewji SA (2017) Comparison of monoenergetic photon organ dose rate coefficients for the female stylized and voxel phantoms submerged in air. Radiat Prot Dosim 175(3):336-43

International Commission on Radiological Protection (1996) ICRP Publication 74: Conversion coefficients for use in radiological protection against external radiation. In: Annals of the ICRP 26 (3-4)

International Commission on Radiological Protection (2002) ICRP Publication 89: Basic anatomical and physiological data for use in radiological protection: reference values. In: Annals of the ICRP 32

International Commission on Radiological Protection (2007) ICRP Publication 103: The 2007 Recommendations of the International Commission on Radiological Protection. In: Annals of the ICRP 37

International Commission on Radiological Protection (2009) ICRP Publication 110: Adult reference computational phantoms. In: Annals of the ICRP 39

International Commission on Radiological Protection (2010) ICRP Publication 116: Conversion coefficients for radiological protection quantities for external radiation exposures. In: Annals of the ICRP 40

Pelowitz DB, Fallgren AJ, McMath GE (2014) MCNP6 User's Manual, Code Version 6.1.1 beta. Los Alamos National Laboratory, Los Alamos

Vazquez JA, Caracappa PF, Xu XG (2014) Development of posture- specific computational phantoms using motion capture technology and application to radiation dose-reconstruction for the 1999 Tokai-Mura nuclear criticality accident. Phys Med Biol 59(18):5277-5286

Xu XG (2014) An exponential growth of computational phantom research in radiation protection, imaging, and radiotherapy: a review of the fifty-year history. Phys Med Biol 59 (18):R233-R302

List of Tables

Table 4 Effective dose coefficients (pSv cm2) for AP, PA, LLAT, and RLAT irradiation geometries for upright, 45°, and 90° bent postures for neutron energies of 1 □ 10-9 to *20* MeV. AP – antero – posterior; PA – postero – anterior; LLAT – left lateral; RLAT – right lateral

Table 2 Ratios of sex-averaged organ absorbed dose coefficients (45º bent/upright) for AP, PA, LLAT and RLAT irradiation geometries for selected neutron energies from 0.01 MeV to 20 MeV. AP – antero – posterior; PA – postero – anterior; LLAT – left lateral; RLAT – right lateral

Energy	45º bent/upright								
	AP								
Organs/tissues	0.01 MeV	0.05 MeV	0.1 MeV	0.5 MeV	1 MeV	5 MeV	10 MeV	15 MeV	20 MeV
Gonads	0.72	0.66	0.72	0.71	0.73	0.89	0.95	1.03	1.12
Bone Marrow	0.82	0.82	0.83	0.85	0.88	0.91	0.92	0.91	0.96
Colon	0.61	0.60	0.59	0.55	0.54	0.75	0.84	0.92	1.04
Lungs	0.71	0.71	0.68	0.62	0.62	0.83	0.90	0.97	1.07
Stomach	0.61	0.61	0.60	0.58	0.60	0.83	0.91	0.99	1.11
Urinary bladder	0.69	0.67	0.64	0.63	0.65	0.87	0.94	1.02	1.13
Breast	0.81	0.83	0.85	0.93	0.95	1.04	1.07	1.12	1.16
Liver	0.58	0.58	0.57	0.56	0.58	0.79	0.87	0.94	1.05
Esophagus	0.73	0.78	0.71	0.72	0.69	0.74	0.82	0.87	0.97
Thyroid	0.83	0.63	0.48	0.24	0.23	0.45	0.56	0.63	0.74
Skin	0.76	0.87	0.92	0.97	0.98	0.98	1.02	1.09	1.16
Bone Surface	0.85	0.85	0.85	0.88	0.91	0.95	0.96	0.95	0.98
Adrenals	0.58	0.66	0.60	0.66	0.64	0.64	0.72	0.75	0.84
Brain	1.49	1.52	1.55	1.59	1.59	1.26	1.23	1.24	1.27
Extrathoracic airways	0.87	0.86	0.75	0.40	0.35	0.51	0.62	0.69	0.78
Small intestine	0.62	0.61	0.61	0.56	0.55	0.73	0.82	0.89	1.01
Kidneys	0.57	0.57	0.57	0.57	0.55	0.56	0.66	0.72	0.83
Muscle	0.67	0.69	0.70	0.75	0.78	0.86	0.91	0.95	1.04
Pancreas	0.59	0.59	0.59	0.55	0.53	0.67	0.76	0.84	0.95
Spleen	0.51	0.51	0.54	0.51	0.50	0.62	0.72	0.78	0.90
Thymus	0.80	0.75	0.70	0.70	0.73	0.95	1.00	1.07	1.15
Uterus/Prostate	0.63	0.66	0.67	0.56	0.55	0.75	0.84	0.90	1.01
Eyes	0.88	0.81	0.79	0.84	0.86	0.99	1.04	1.10	1.14
Gall bladder	0.60	0.62	0.67	0.56	0.56	0.77	0.87	0.93	1.06
Heart	0.68	0.66	0.66	0.62	0.63	0.83	0.91	0.98	1.08
Oral mucosa	0.88	0.85	0.80	0.68	0.68	0.85	0.91	0.96	1.03
Salivary glands	0.90	0.85	0.84	0.67	0.66	0.84	0.90	0.95	1.03

Energy	45º bent/upright								
	PA								
Organs/tissues	0.01 MeV	0.05 MeV	0.1 MeV	0.5 MeV	1 MeV	5 MeV	10 MeV	15 MeV	20 MeV
Gonads	0.92	1.00	1.03	1.15	1.23	1.03	1.03	1.07	1.14
Bone Marrow	0.72	0.71	0.71	0.72	0.75	0.89	0.92	0.92	0.97
Colon	0.67	0.68	0.69	0.68	0.68	0.72	0.79	0.85	0.96
Lungs	0.61	0.60	0.58	0.55	0.57	0.76	0.85	0.92	1.02
Stomach	0.61	0.59	0.59	0.55	0.56	0.58	0.68	0.73	0.85
Urinary bladder	0.96	0.92	0.92	1.03	1.15	1.12	1.10	1.12	1.21
Breast	0.78	0.74	0.76	0.64	0.73	0.40	0.48	0.52	0.59
Liver	0.55	0.55	0.55	0.52	0.53	0.68	0.76	0.81	0.92
Esophagus	0.60	0.61	0.60	0.54	0.53	0.72	0.80	0.87	0.96
Thyroid	0.59	0.58	0.56	0.38	0.32	0.47	0.60	0.68	0.80
Skin	0.65	0.75	0.78	0.83	0.85	0.87	0.92	1.00	1.08
Bone Surface	0.78	0.76	0.76	0.80	0.82	0.94	0.95	0.96	1.00
Adrenals	0.61	0.60	0.63	0.56	0.58	0.83	0.91	0.96	1.09
Brain	0.69	0.67	0.66	0.66	0.67	0.87	0.95	1.02	1.11
Extrathoracic airways	0.58	0.57	0.51	0.41	0.40	0.62	0.73	0.83	0.93
Small intestine	0.62	0.62	0.62	0.58	0.56	0.66	0.76	0.82	0.93
Kidneys	0.61	0.61	0.58	0.61	0.64	0.89	0.95	1.03	1.13
Muscle	0.65	0.66	0.67	0.70	0.72	0.82	0.88	0.92	1.00
Pancreas	0.59	0.60	0.58	0.55	0.53	0.67	0.76	0.82	0.93
Spleen	0.55	0.54	0.55	0.52	0.54	0.8	0.88	0.96	1.07
Thymus	0.75	0.69	0.72	0.66	0.72	0.57	0.64	0.66	0.78
Uterus/Prostate	0.93	0.96	1.12	1.55	1.76	1.25	1.19	1.19	1.24
Eyes	0.77	0.81	0.73	0.73	0.74	0.58	0.67	0.72	0.85
Gall bladder	0.66	0.60	0.63	0.61	0.59	0.59	0.71	0.74	0.83
Heart	0.64	0.64	0.63	0.58	0.57	0.57	0.66	0.72	0.83
Oral mucosa	0.67	0.67	0.66	0.55	0.51	0.56	0.66	0.73	0.82
Salivary glands	0.65	0.66	0.65	0.52	0.45	0.53	0.64	0.70	0.80

Energy	45º bent/upright								
	LLAT								
Organs/tissues	0.01 MeV	0.05 MeV	0.1 MeV	0.5 MeV	1 MeV	5 MeV	10 MeV	15 MeV	20 MeV
Gonads	1.76	1.61	1.45	1.01	0.95	1.08	1.14	1.18	1.24
Bone Marrow	1.21	1.20	1.19	1.15	1.14	1.10	1.10	1.07	1.09
Colon	1.79	1.79	1.81	2.02	2.12	1.79	1.64	1.58	1.62

Lungs	1.70	1.69	1.73	2.10	2.19	1.71	1.58	1.55	1.57
Stomach	1.88	1.92	1.91	1.82	1.79	1.45	1.38	1.38	1.40
Urinary bladder	1.55	1.56	1.63	1.53	1.35	1.21	1.21	1.23	1.28
Breast	1.47	1.31	1.21	1.10	1.07	1.08	1.09	1.11	1.13
Liver	1.74	1.69	1.70	1.67	1.61	1.47	1.43	1.40	1.46
Esophagus	1.55	1.50	1.58	1.72	1.70	1.85	1.69	1.63	1.66
Thyroid	1.08	1.07	1.08	1.02	1.00	1.01	1.05	1.11	1.15
Skin	1.38	1.31	1.28	1.20	1.18	1.08	1.10	1.13	1.16
Bone Surface	1.10	1.10	1.09	1.07	1.07	1.09	1.09	1.07	1.09
Adrenals	1.72	1.63	1.79	1.57	1.63	1.26	1.22	1.22	1.25
Brain	1.13	1.11	1.09	1.04	1.02	1.03	1.06	1.10	1.16
Extrathoracic airways	1.09	1.15	1.08	1.02	1.03	1.03	1.06	1.11	1.17
Small intestine	1.80	1.78	1.79	1.86	1.92	1.72	1.60	1.55	1.59
Kidneys	1.69	1.70	1.66	1.41	1.32	1.14	1.14	1.15	1.20
Muscle	1.66	1.65	1.65	1.59	1.54	1.25	1.23	1.23	1.26
Pancreas	1.94	1.97	2.11	2.52	2.70	2.20	1.92	1.82	1.83
Spleen	2.16	2.11	2.16	2.74	2.84	1.86	1.66	1.61	1.60
Thymus	1.42	1.55	1.42	1.30	1.11	0.95	0.97	0.99	1.04
Uterus/Prostate	1.48	1.55	1.55	1.59	1.47	1.50	1.42	1.39	1.44
Eyes	0.97	1.01	0.99	1.02	1.02	1.04	1.07	1.12	1.17
Gall bladder	1.53	1.79	1.74	1.65	1.75	1.61	1.51	1.44	1.53
Heart	1.75	1.71	1.74	1.77	1.77	1.50	1.44	1.42	1.46
Oral mucosa	1.09	1.07	1.08	1.04	1.03	1.03	1.06	1.10	1.15
Salivary glands	1.08	1.07	1.06	1.05	1.02	1.04	1.06	1.09	1.15

Energy	45º bent/upright								
	RLAT								
Organs/tissues	0.01 MeV	0.05 MeV	0.1 MeV	0.5 MeV	1 MeV	5 MeV	10 MeV	15 MeV	20 MeV
Gonads	1.59	1.49	1.47	1.10	1.02	1.07	1.15	1.19	1.27
Bone Marrow	1.21	1.20	1.19	1.15	1.14	1.10	1.09	1.07	1.09
Colon	1.78	1.80	1.83	1.92	1.98	1.67	1.56	1.52	1.57
Lungs	1.68	1.69	1.74	2.11	2.19	1.72	1.59	1.56	1.57
Stomach	1.78	1.75	1.75	1.71	1.68	1.46	1.41	1.39	1.43
Urinary bladder	1.54	1.52	1.47	1.49	1.36	1.21	1.21	1.22	1.26
Breast	1.47	1.29	1.21	1.09	1.07	1.08	1.09	1.11	1.13
Liver	2.07	2.16	2.27	2.75	2.77	1.70	1.54	1.50	1.49
Esophagus	1.53	1.54	1.56	1.61	1.71	1.82	1.67	1.60	1.63
Thyroid	1.13	1.08	1.13	1.01	1.01	1.01	1.05	1.10	1.15
Skin	1.38	1.31	1.27	1.20	1.18	1.08	1.10	1.13	1.16
Bone Surface	1.10	1.10	1.09	1.07	1.07	1.09	1.09	1.07	1.09
Adrenals	1.70	1.72	1.67	1.53	1.51	1.25	1.21	1.22	1.26
Brain	1.12	1.11	1.09	1.03	1.02	1.03	1.06	1.10	1.16
Extrathoracic airways	1.15	1.13	1.04	1.03	1.03	1.04	1.07	1.11	1.18
Small intestine	1.76	1.78	1.80	1.86	1.90	1.72	1.61	1.56	1.60
Kidneys	1.70	1.71	1.63	1.43	1.33	1.14	1.14	1.15	1.20
Muscle	1.62	1.62	1.61	1.53	1.48	1.23	1.21	1.22	1.26
Pancreas	1.76	1.74	1.75	1.73	1.75	1.93	1.78	1.70	1.75
Spleen	1.57	1.71	1.63	1.63	1.60	1.59	1.52	1.49	1.55
Thymus	1.35	1.36	1.43	1.20	1.11	0.96	0.98	1.01	1.05
Uterus/Prostate	1.52	1.48	1.48	1.46	1.44	1.48	1.43	1.39	1.45
Eyes	1.06	1.04	1.04	1.02	1.02	1.04	1.07	1.13	1.18
Gall bladder	1.80	1.80	1.84	1.75	1.86	1.67	1.58	1.46	1.49
Heart	1.71	1.69	1.75	1.87	1.87	1.59	1.49	1.47	1.50
Oral mucosa	1.10	1.10	1.08	1.04	1.03	1.03	1.06	1.10	1.15
Salivary glands	1.09	1.10	1.04	1.05	1.04	1.03	1.06	1.09	1.15

Table 3 Ratios of sex-averaged organ absorbed dose coefficients (90º bent/upright) for AP, PA, LLAT, and RLAT irradiation geometries for selected neutron energies from 0.01 MeV to 20 MeV. AP – antero – posterior; PA – postero – anterior; LLAT – left lateral; RLAT – right lateral

Energy	90º bent/upright								
	AP								
Organs/tissues	0.01 MeV	0.05 MeV	0.1 MeV	0.5 MeV	1 MeV	5 MeV	10 MeV	15 MeV	20 MeV
Gonads	0.23	0.19	0.15	0.09	0.07	0.05	0.06	0.07	0.08
Bone Marrow	0.50	0.50	0.50	0.52	0.55	0.60	0.61	0.61	0.63
Colon	0.08	0.08	0.07	0.05	0.04	0.03	0.06	0.08	0.11
Lungs	0.25	0.24	0.23	0.21	0.22	0.41	0.48	0.52	0.58
Stomach	0.08	0.07	0.07	0.04	0.04	0.09	0.15	0.19	0.25
Urinary bladder	0.14	0.13	0.11	0.05	0.05	0.03	0.04	0.04	0.05
Breast	0.30	0.33	0.36	0.48	0.51	0.76	0.83	0.90	0.96
Liver	0.09	0.08	0.08	0.05	0.04	0.12	0.18	0.23	0.28
Esophagus	0.24	0.23	0.23	0.20	0.18	0.18	0.24	0.27	0.31
Thyroid	0.35	0.27	0.20	0.07	0.06	0.16	0.25	0.31	0.37
Skin	0.29	0.29	0.29	0.31	0.33	0.40	0.43	0.46	0.50
Bone Surface	0.61	0.61	0.61	0.64	0.68	0.75	0.75	0.76	0.78
Adrenals	0.12	0.12	0.12	0.10	0.11	0.11	0.14	0.17	0.20
Brain	1.34	1.48	1.61	1.86	1.90	1.34	1.24	1.19	1.15
Extrathoracic airways	0.44	0.42	0.37	0.17	0.16	0.33	0.42	0.47	0.53
Small intestine	0.08	0.08	0.07	0.04	0.04	0.03	0.05	0.07	0.10
Kidneys	0.10	0.10	0.09	0.08	0.08	0.10	0.15	0.18	0.22
Muscle	0.19	0.18	0.18	0.17	0.18	0.21	0.24	0.26	0.29
Pancreas	0.09	0.08	0.08	0.06	0.06	0.09	0.14	0.17	0.21
Spleen	0.10	0.09	0.09	0.08	0.07	0.23	0.32	0.35	0.42
Thymus	0.16	0.14	0.12	0.06	0.05	0.10	0.16	0.21	0.25
Uterus/Prostate	0.13	0.13	0.12	0.07	0.06	0.02	0.03	0.04	0.05
Eyes	0.36	0.23	0.18	0.19	0.22	0.61	0.69	0.75	0.80
Gall bladder	0.07	0.07	0.07	0.05	0.04	0.04	0.07	0.10	0.13
Heart	0.13	0.13	0.12	0.07	0.07	0.10	0.14	0.18	0.22
Oral mucosa	0.35	0.34	0.30	0.17	0.18	0.44	0.55	0.61	0.67
Salivary glands	0.36	0.36	0.33	0.19	0.21	0.43	0.54	0.59	0.66

Energy	90º bent/upright								
	PA								
Organs/tissues	0.01 MeV	0.05 MeV	0.1 MeV	0.5 MeV	1 MeV	5 MeV	10 MeV	15 MeV	20 MeV
Gonads	0.72	0.80	0.91	1.43	1.60	0.94	0.88	0.86	0.85
Bone Marrow	0.38	0.35	0.33	0.29	0.28	0.42	0.45	0.48	0.50
Colon	0.20	0.20	0.21	0.21	0.21	0.27	0.34	0.38	0.45
Lungs	0.11	0.10	0.09	0.04	0.03	0.02	0.04	0.05	0.07
Stomach	0.16	0.15	0.15	0.11	0.12	0.07	0.10	0.13	0.17
Urinary bladder	0.60	0.59	0.58	0.68	0.79	0.95	0.94	0.94	0.97
Breast	0.43	0.41	0.41	0.42	0.46	0.32	0.37	0.36	0.39
Liver	0.11	0.10	0.10	0.06	0.05	0.04	0.07	0.10	0.14
Esophagus	0.06	0.06	0.06	0.04	0.03	0.02	0.04	0.05	0.08
Thyroid	0.07	0.07	0.06	0.03	0.02	0.01	0.02	0.03	0.04
Skin	0.15	0.11	0.10	0.09	0.10	0.17	0.21	0.26	0.30
Bone Surface	0.57	0.55	0.53	0.55	0.57	0.70	0.72	0.73	0.75
Adrenals	0.04	0.04	0.04	0.02	0.01	0.02	0.04	0.07	0.10
Brain	0.04	0.04	0.03	0.01	0.01	0.02	0.02	0.03	0.04
Extrathoracic airways	0.04	0.04	0.04	0.02	0.01	0.01	0.02	0.03	0.03
Small intestine	0.12	0.12	0.12	0.09	0.08	0.16	0.25	0.31	0.38
Kidneys	0.04	0.03	0.03	0.01	0.01	0.03	0.07	0.10	0.15
Muscle	0.16	0.15	0.14	0.11	0.10	0.18	0.23	0.27	0.31
Pancreas	0.08	0.08	0.07	0.05	0.04	0.04	0.09	0.12	0.17
Spleen	0.05	0.05	0.05	0.02	0.02	0.02	0.04	0.07	0.10
Thymus	0.21	0.19	0.19	0.16	0.17	0.08	0.09	0.10	0.12
Uterus/Prostate	0.48	0.51	0.57	0.89	1.05	1.02	0.99	0.99	1.02
Eyes	0.17	0.17	0.17	0.19	0.25	0.11	0.09	0.10	0.10
Gall bladder	0.13	0.13	0.12	0.09	0.09	0.07	0.13	0.17	0.22
Heart	0.15	0.14	0.13	0.10	0.09	0.04	0.06	0.08	0.11
Oral mucosa	0.08	0.08	0.07	0.05	0.05	0.03	0.04	0.05	0.06
Salivary glands	0.07	0.07	0.06	0.04	0.04	0.03	0.03	0.04	0.05

Energy	90º bent/upright								
	LLAT								
Organs/tissues	0.01 MeV	0.05 MeV	0.1 MeV	0.5 MeV	1 MeV	5 MeV	10 MeV	15 MeV	20 MeV
Gonads	1.63	1.53	1.48	1.02	0.90	0.95	1.00	1.03	1.04
Bone Marrow	1.21	1.21	1.20	1.16	1.15	1.09	1.08	1.07	1.06
Colon	1.76	1.73	1.75	1.96	2.07	1.76	1.56	1.48	1.41

Lungs	1.50	1.50	1.56	1.94	2.03	1.61	1.45	1.38	1.33
Stomach	1.82	1.83	1.82	1.78	1.77	1.43	1.33	1.27	1.22
Urinary bladder	1.66	1.62	1.64	1.50	1.42	1.23	1.19	1.17	1.13
Breast	1.17	0.88	0.73	0.55	0.53	0.72	0.78	0.81	0.83
Liver	1.66	1.66	1.65	1.62	1.58	1.46	1.38	1.34	1.30
Esophagus	1.37	1.40	1.44	1.55	1.64	1.81	1.61	1.52	1.46
Thyroid	1.05	1.03	1.04	1.01	1.01	1.00	1.00	1.00	0.99
Skin	1.33	1.27	1.24	1.17	1.16	1.04	1.03	1.01	0.99
Bone Surface	1.14	1.14	1.13	1.09	1.08	1.08	1.09	1.08	1.07
Adrenals	1.59	1.47	1.60	1.51	1.48	1.24	1.18	1.14	1.11
Brain	1.02	1.01	1.01	1.01	1.01	1.00	1.00	1.00	1.00
Extrathoracic airways	1.04	1.05	1.05	1.00	1.01	1.00	1.00	1.00	1.00
Small intestine	1.73	1.73	1.73	1.81	1.87	1.69	1.53	1.45	1.39
Kidneys	1.56	1.56	1.56	1.37	1.30	1.11	1.08	1.06	1.04
Muscle	1.57	1.58	1.58	1.54	1.51	1.22	1.17	1.15	1.12
Pancreas	1.86	1.85	1.93	2.38	2.64	2.15	1.84	1.70	1.61
Spleen	1.95	1.97	2.03	2.64	2.79	1.82	1.57	1.46	1.37
Thymus	1.20	1.22	1.21	0.96	0.80	0.56	0.62	0.65	0.66
Uterus/Prostate	1.46	1.46	1.49	1.53	1.45	1.48	1.38	1.34	1.30
Eyes	1.01	1.03	1.02	1.01	1.00	1.01	1.01	1.01	1.01
Gall bladder	1.65	1.77	1.76	1.66	1.63	1.61	1.48	1.43	1.38
Heart	1.53	1.56	1.53	1.60	1.62	1.45	1.35	1.31	1.27
Oral mucosa	1.03	1.03	1.02	1.02	1.01	1.01	1.01	1.01	1.01
Salivary glands	1.02	1.02	1.02	1.02	1.01	1.01	1.01	1.01	1.01

Energy	90º bent/upright								
	RLAT								
Organs/tissues	0.01 MeV	0.05 MeV	0.1 MeV	0.5 MeV	1 MeV	5 MeV	10 MeV	15 MeV	20 MeV
Gonads	1.58	1.62	1.55	1.05	0.90	0.95	1.00	1.03	1.03
Bone Marrow	1.21	1.21	1.20	1.16	1.15	1.09	1.08	1.08	1.06
Colon	1.75	1.74	1.76	1.87	1.94	1.65	1.50	1.42	1.36
Lungs	1.51	1.52	1.56	1.95	2.04	1.62	1.46	1.39	1.33
Stomach	1.73	1.72	1.71	1.70	1.64	1.47	1.37	1.32	1.28
Urinary bladder	1.62	1.59	1.58	1.50	1.42	1.22	1.19	1.17	1.13
Breast	1.16	0.88	0.73	0.55	0.53	0.72	0.78	0.81	0.83
Liver	1.95	2.01	2.14	2.67	2.74	1.67	1.48	1.39	1.31
Esophagus	1.34	1.33	1.39	1.55	1.60	1.76	1.58	1.50	1.44
Thyroid	1.00	1.05	1.03	1.01	1.00	1.00	1.00	1.01	1.00
Skin	1.32	1.27	1.24	1.17	1.16	1.04	1.03	1.01	0.99
Bone Surface	1.14	1.14	1.13	1.09	1.08	1.08	1.09	1.08	1.07
Adrenals	1.48	1.57	1.62	1.54	1.48	1.23	1.16	1.14	1.11
Brain	1.02	1.02	1.01	1.01	1.01	1.00	1.00	1.00	1.00
Extrathoracic airways	1.05	1.04	1.04	1.02	1.01	1.00	1.00	1.00	1.00
Small intestine	1.71	1.72	1.72	1.80	1.85	1.70	1.53	1.46	1.39
Kidneys	1.56	1.56	1.53	1.37	1.30	1.11	1.08	1.06	1.04
Muscle	1.54	1.54	1.54	1.49	1.45	1.20	1.16	1.14	1.11
Pancreas	1.60	1.64	1.64	1.64	1.67	1.90	1.71	1.61	1.55
Spleen	1.57	1.57	1.58	1.60	1.52	1.56	1.47	1.40	1.36
Thymus	1.24	1.25	1.20	0.98	0.83	0.57	0.62	0.65	0.66
Uterus/Prostate	1.51	1.50	1.50	1.47	1.44	1.48	1.39	1.34	1.31
Eyes	1.03	1.00	1.04	1.04	1.01	1.01	1.01	1.01	1.01
Gall bladder	1.72	1.66	1.74	1.78	1.77	1.67	1.52	1.43	1.39
Heart	1.54	1.54	1.57	1.69	1.74	1.53	1.41	1.35	1.30
Oral mucosa	1.03	1.03	1.03	1.01	1.01	1.01	1.01	1.01	1.01
Salivary glands	1.03	1.03	1.01	1.01	1.01	1.01	1.01	1.01	1.01

Table 4 Effective dose coefficients (pSv cm^2) for AP, PA, LLAT, and RLAT irradiation geometries for upright, 45°, and 90° bent postures for neutron energies of $1 \cdot 10^{-9}$ to 20 MeV. AP – antero – posterior; PA – postero – anterior; LLAT – left lateral; RLAT – right lateral

Irradiation Geometry	Neutron Energy (MeV)	Upright (pSv-cm^2)	Error (%)	45° Bent (pSv-cm^2)	Error (%)	Relative difference to upright (%)	90° Bent (pSv-cm^2)	Error (%)	Relative difference to upright (%)
AP	$1.0 \cdot 10^{-9}$	3.11	0.12	2.05	0.11	-34.05	0.89	0.23	-71.29
	$1.0 \cdot 10^{-8}$	3.61	0.09	2.33	0.11	-35.60	0.97	0.30	-73.07
	$2.5 \cdot 10^{-8}$	4.19	0.08	2.67	0.10	-36.29	1.09	0.30	-73.98
	$1.0 \cdot 10^{-7}$	5.37	0.07	3.44	0.09	-35.95	1.29	0.27	-76.00
	$2.0 \cdot 10^{-7}$	5.97	0.06	3.82	0.08	-35.98	1.39	0.26	-76.63
	$5.0 \cdot 10^{-7}$	6.74	0.06	4.31	0.08	-36.04	1.53	0.25	-77.31
	$1.0 \cdot 10^{-6}$	7.15	0.06	4.62	0.07	-35.41	1.59	0.25	-77.72
	$2.0 \cdot 10^{-6}$	7.45	0.06	4.82	0.07	-35.36	1.64	0.24	-78.02
	$5.0 \cdot 10^{-6}$	7.75	0.10	4.98	0.07	-35.77	1.69	0.25	-78.18
	$1.0 \cdot 10^{-5}$	7.84	0.05	5.09	0.06	-35.17	1.71	0.24	-78.22
	$2.0 \cdot 10^{-5}$	7.88	0.05	5.12	0.07	-35.10	1.72	0.23	-78.18
	$5.0 \cdot 10^{-5}$	7.90	0.05	5.14	0.07	-35.00	1.70	0.24	-78.46
	$1.0 \cdot 10^{-4}$	7.86	0.05	5.13	0.05	-34.73	1.71	0.23	-78.19
	$2.0 \cdot 10^{-4}$	7.82	0.05	5.11	0.07	-34.65	1.70	0.23	-78.31
	$5.0 \cdot 10^{-4}$	7.78	0.05	5.07	0.07	-34.84	1.67	0.24	-78.50
	0.001	7.85	0.05	5.04	0.05	-35.85	1.67	0.23	-78.73
	0.002	8.32	0.09	5.05	0.05	-39.29	1.58	0.24	-81.03
	0.005	9.04	0.05	5.35	0.05	-40.78	1.67	0.24	-81.51
	0.01	10.79	0.03	6.12	0.05	-43.27	1.92	0.09	-82.22
	0.02	14.39	0.05	8.21	0.05	-42.94	2.58	0.23	-82.07
	0.03	18.46	0.09	10.53	0.05	-42.96	3.31	0.24	-82.05
	0.05	26.54	0.03	15.36	0.05	-42.13	4.88	0.09	-81.60
	0.07	34.60	0.05	20.24	0.05	-41.52	6.45	0.24	-81.36
	0.1	47.20	0.03	27.88	0.05	-40.92	9.28	0.09	-80.34
	0.15	68.43	0.04	40.16	0.05	-41.32	13.41	0.23	-80.40
	0.2	88.37	0.04	51.99	0.05	-41.17	17.40	0.24	-80.32
	0.3	121.18	0.04	74.11	0.04	-38.84	25.13	0.23	-79.26
	0.5	176.69	0.02	116.21	0.04	-34.23	39.26	0.08	-77.78
	0.7	228.81	0.03	153.98	0.03	-32.70	52.23	0.20	-77.17
	0.9	269.08	0.03	184.04	0.03	-31.61	62.54	0.20	-76.76
	1	267.78	0.02	179.17	0.04	-33.09	62.43	0.07	-76.69
	1.2	319.68	0.04	218.55	0.03	-31.64	74.66	0.18	-76.65
	1.5	356.67	0.03	249.51	0.03	-30.04	85.01	0.17	-76.16
	2	392.69	0.02	286.77	0.02	-26.97	98.52	0.14	-74.91
	3	432.58	0.01	335.71	0.02	-22.39	118.40	0.11	-72.63
	4	453.59	0.02	360.55	0.02	-20.51	127.52	0.10	-71.89
	5	447.34	0.01	366.73	0.01	-18.02	136.05	0.03	-69.59
	7	449.18	0.01	380.79	0.01	-15.23	147.65	0.08	-67.13
	8	446.27	0.01	382.82	0.01	-14.22	151.93	0.07	-65.95
	9	444.21	0.01	381.45	0.02	-14.13	151.80	0.07	-65.83
	10	436.43	0.01	375.81	0.02	-13.89	151.14	0.03	-65.37
	12	429.55	0.02	374.57	0.02	-12.80	152.66	0.07	-64.46
	14	419.46	0.02	373.74	0.02	-10.90	157.45	0.08	-62.46
	15	416.91	0.01	374.49	0.02	-10.18	158.65	0.03	-61.95
	16	357.43	0.02	367.35	0.02	2.78	159.69	0.08	-55.32
	18	348.11	0.02	365.38	0.02	4.96	163.67	0.08	-52.98
	20	338.65	0.02	359.32	0.03	6.10	164.08	0.03	-51.55
PA	$1.0 \cdot 10^{-9}$	2.22	0.13	1.41	0.12	-36.79	0.74	0.31	-66.62
	$1.0 \cdot 10^{-8}$	2.62	0.16	1.60	0.12	-38.98	0.80	0.41	-69.43
	$2.5 \cdot 10^{-8}$	3.04	0.15	1.84	0.11	-39.54	0.88	0.41	-71.08
	$1.0 \cdot 10^{-7}$	3.87	0.13	2.40	0.09	-38.13	1.07	0.37	-72.30
	$2.0 \cdot 10^{-7}$	4.31	0.12	2.68	0.09	-37.88	1.16	0.35	-73.15
	$5.0 \cdot 10^{-7}$	4.92	0.11	3.08	0.08	-37.48	1.30	0.34	-73.59
	$1.0 \cdot 10^{-6}$	5.23	0.11	3.28	0.08	-37.26	1.38	0.34	-73.57
	$2.0 \cdot 10^{-6}$	5.50	0.11	3.46	0.08	-37.00	1.42	0.33	-74.14
	$5.0 \cdot 10^{-6}$	5.77	0.10	3.61	0.08	-37.35	1.48	0.31	-74.38
	$1.0 \cdot 10^{-5}$	5.86	0.10	3.68	0.08	-37.10	1.51	0.32	-74.18
	$2.0 \cdot 10^{-5}$	5.92	0.10	3.75	0.07	-36.65	1.52	0.33	-74.34

	$5.0\cdot10^{-5}$	5.96	0.10	3.78	0.07	-36.52	1.52	0.31	-74.49
	$1.0\cdot10^{-4}$	5.95	0.10	3.78	0.07	-36.45	1.53	0.32	-74.25
	$2.0\cdot10^{-4}$	5.99	0.10	3.79	0.07	-36.67	1.54	0.31	-74.23
	$5.0\cdot10^{-4}$	6.01	0.10	3.79	0.07	-36.91	1.51	0.32	-74.85
	0.001	6.21	0.10	3.78	0.07	-39.09	1.51	0.33	-75.71
	0.002	6.61	0.10	3.83	0.07	-42.06	1.52	0.32	-77.01
	0.005	7.29	0.10	4.03	0.07	-44.69	1.59	0.33	-78.15
	0.01	8.92	0.04	4.59	0.07	-48.60	1.81	0.12	-79.67
	0.02	11.68	0.10	6.04	0.07	-48.26	2.35	0.32	-79.91
	0.03	15.02	0.10	7.63	0.07	-49.20	2.95	0.32	-80.37
	0.05	21.04	0.04	10.77	0.07	-48.80	4.13	0.12	-80.38
	0.07	26.82	0.09	13.72	0.07	-48.83	5.29	0.32	-80.27
	0.1	35.66	0.03	18.01	0.07	-49.49	6.87	0.12	-80.73
	0.15	50.69	0.05	24.50	0.07	-51.67	9.35	0.32	-81.56
	0.2	63.24	0.08	30.62	0.06	-51.59	11.53	0.31	-81.77
	0.3	81.27	0.08	41.64	0.06	-48.77	15.77	0.31	-80.59
	0.5	106.37	0.02	62.17	0.05	-41.55	23.51	0.11	-77.89
	0.7	138.38	0.06	82.73	0.05	-40.21	30.45	0.30	-77.99
	0.9	161.16	0.05	98.30	0.04	-39.00	36.05	0.28	-77.63
	1	152.04	0.02	91.30	0.04	-39.95	33.90	0.11	-77.71
	1.2	197.79	0.04	118.83	0.04	-39.92	42.93	0.27	-78.29
	1.5	229.41	0.02	139.96	0.03	-38.99	49.84	0.26	-78.28
	2	262.18	0.03	167.94	0.02	-35.94	59.23	0.23	-77.41
	3	311.02	0.02	211.27	0.02	-32.07	74.04	0.18	-76.20
	4	335.73	0.02	232.79	0.02	-30.66	82.42	0.14	-75.45
	5	346.85	0.01	249.67	0.02	-28.02	88.99	0.05	-74.34
	7	366.33	0.02	273.93	0.02	-25.22	100.86	0.11	-72.47
	8	372.02	0.02	282.16	0.02	-24.15	105.76	0.10	-71.57
	9	371.39	0.02	282.55	0.02	-23.92	106.25	0.10	-71.39
	10	366.67	0.01	280.33	0.02	-23.55	106.19	0.04	-71.04
	12	367.57	0.02	284.63	0.02	-22.56	109.45	0.10	-70.22
	14	368.06	0.02	291.80	0.02	-20.72	114.95	0.09	-68.77
	15	368.76	0.01	294.46	0.02	-20.15	116.85	0.03	-68.31
	16	310.68	0.02	292.47	0.02	-5.86	117.99	0.10	-62.02
	18	309.38	0.02	296.04	0.02	-4.31	122.63	0.10	-60.36
	20	303.69	0.02	293.93	0.03	-3.21	123.56	0.04	-59.31
LLAT	$1.0\cdot10^{-9}$	0.91	0.23	1.05	0.16	15.07	1.06	0.20	16.82
	$1.0\cdot10^{-8}$	1.02	0.18	1.22	0.15	19.77	1.22	0.25	19.72
	$2.5\cdot10^{-8}$	1.19	0.17	1.43	0.14	20.49	1.44	0.23	21.37
	$1.0\cdot10^{-7}$	1.48	0.14	1.93	0.12	30.18	1.92	0.19	29.99
	$2.0\cdot10^{-7}$	1.65	0.13	2.17	0.11	31.95	2.17	0.19	31.83
	$5.0\cdot10^{-7}$	1.86	0.12	2.51	0.10	35.52	2.52	0.17	35.80
	$1.0\cdot10^{-6}$	1.97	0.12	2.72	0.10	38.14	2.71	0.17	37.85
	$2.0\cdot10^{-6}$	2.03	0.12	2.87	0.10	41.18	2.88	0.16	41.58
	$5.0\cdot10^{-6}$	2.14	0.19	3.00	0.09	40.28	3.03	0.16	41.58
	$1.0\cdot10^{-5}$	2.17	0.11	3.08	0.09	42.27	3.10	0.15	43.11
	$2.0\cdot10^{-5}$	2.18	0.11	3.12	0.09	43.47	3.13	0.15	43.99
	$5.0\cdot10^{-5}$	2.19	0.11	3.15	0.09	44.31	3.13	0.15	43.40
	$1.0\cdot10^{-4}$	2.19	0.11	3.14	0.09	43.71	3.16	0.15	44.66
	$2.0\cdot10^{-4}$	2.18	0.11	3.13	0.09	43.61	3.17	0.15	45.59
	$5.0\cdot10^{-4}$	2.18	0.11	3.12	0.09	43.10	3.14	0.15	43.83
	0.001	2.22	0.11	3.09	0.09	39.30	3.12	0.15	40.53
	0.002	2.37	0.18	3.12	0.09	31.78	3.17	0.15	33.73
	0.005	2.61	0.11	3.28	0.09	25.61	3.34	0.15	27.91
	0.01	3.20	0.07	3.76	0.09	17.78	3.80	0.06	18.81
	0.02	4.25	0.11	5.00	0.09	17.49	5.02	0.15	18.03
	0.03	5.55	0.11	6.37	0.09	14.62	6.33	0.15	13.92
	0.05	8.05	0.06	9.14	0.09	13.49	9.01	0.05	11.98
	0.7	10.56	0.10	11.91	0.08	12.81	11.73	0.14	11.07
	0.1	14.60	0.06	16.12	0.08	10.40	15.47	0.05	5.92
	0.15	21.85	0.16	22.90	0.08	4.78	21.51	0.13	-1.55
	0.2	28.76	0.09	29.48	0.07	2.50	27.33	0.13	-4.95
	0.3	39.22	0.08	41.93	0.07	6.89	38.50	0.12	-1.83
	0.5	55.28	0.05	67.36	0.06	21.86	60.81	0.04	10.02
	0.07	74.97	0.06	92.29	0.05	23.10	83.18	0.09	10.95
	0.9	90.08	0.06	111.38	0.05	23.65	100.89	0.08	12.00
	1	88.17	0.04	103.23	0.05	17.09	91.61	0.03	3.91
	1.2	114.15	0.05	136.49	0.04	19.56	123.80	0.07	8.45
	1.5	132.97	0.04	161.08	0.03	21.14	146.96	0.06	10.52

	2	155.04	0.03	191.52	0.03	23.53	176.52	0.05	13.86
	3	186.97	0.02	234.87	0.02	25.62	219.43	0.03	17.36
	4	202.52	0.02	256.24	0.02	26.52	241.04	0.03	19.02
	5	218.15	0.01	270.07	0.02	23.80	255.56	0.01	17.15
	7	236.90	0.02	289.96	0.02	22.40	276.56	0.03	16.74
	8	244.02	0.02	296.17	0.02	21.37	283.53	0.03	16.19
	9	244.72	0.02	295.31	0.02	20.67	283.13	0.03	15.70
	10	243.15	0.01	291.99	0.02	20.08	280.14	0.01	15.21
	12	245.36	0.02	293.92	0.02	19.79	282.96	0.03	15.32
	14	251.29	0.02	298.45	0.02	18.77	288.22	0.04	14.70
	15	252.80	0.02	299.87	0.02	18.62	290.05	0.01	14.74
	16	216.12	0.03	297.23	0.02	37.53	287.49	0.04	33.02
	18	219.12	0.03	298.88	0.03	36.40	289.56	0.04	32.15
	20	217.99	0.02	295.66	0.03	35.63	286.85	0.02	31.58
RLAT	$1.0\cdot10^{-9}$	0.83	0.23	0.94	0.16	12.25	0.95	0.20	13.40
	$1.0\cdot10^{-8}$	0.93	0.30	1.08	0.15	16.11	1.09	0.25	17.02
	$2.5\cdot10^{-8}$	1.07	0.27	1.27	0.14	18.44	1.26	0.23	17.93
	$1.0\cdot10^{-7}$	1.33	0.24	1.70	0.12	28.07	1.68	0.20	26.72
	$2.0\cdot10^{-7}$	1.47	0.22	1.91	0.11	29.53	1.90	0.18	28.88
	$5.0\cdot10^{-7}$	1.64	0.21	2.21	0.10	34.53	2.22	0.17	35.20
	$1.0\cdot10^{-6}$	1.76	0.20	2.38	0.10	35.70	2.38	0.16	35.22
	$2.0\cdot10^{-6}$	1.83	0.19	2.50	0.09	36.66	2.51	0.16	37.07
	$5.0\cdot10^{-6}$	1.88	0.19	2.62	0.09	39.45	2.62	0.16	39.52
	$1.0\cdot10^{-5}$	1.92	0.19	2.67	0.09	39.16	2.70	0.15	40.80
	$2.0\cdot10^{-5}$	1.92	0.18	2.70	0.09	40.67	2.68	0.15	39.47
	$5.0\cdot10^{-5}$	1.95	0.18	2.72	0.09	39.47	2.72	0.15	39.44
	$1.0\cdot10^{-4}$	1.95	0.18	2.70	0.09	38.79	2.72	0.15	39.68
	$2.0\cdot10^{-4}$	1.94	0.18	2.71	0.09	39.68	2.72	0.15	40.03
	$5.0\cdot10^{-4}$	1.93	0.18	2.68	0.09	39.18	2.69	0.15	39.40
	0.001	1.97	0.18	2.68	0.09	35.82	2.71	0.15	37.45
	0.002	2.12	0.18	2.68	0.09	26.65	2.72	0.15	28.67
	0.005	2.35	0.18	2.82	0.09	20.25	2.84	0.15	20.80
	0.01	2.90	0.07	3.23	0.09	11.23	3.25	0.06	11.87
	0.02	3.86	0.18	4.33	0.09	12.10	4.29	0.15	11.03
	0.03	5.05	0.17	5.51	0.09	9.07	5.46	0.15	7.93
	0.05	7.35	0.06	7.97	0.09	8.44	7.80	0.05	6.13
	0.07	9.65	0.17	10.45	0.08	8.25	10.15	0.14	5.11
	0.1	13.46	0.06	14.15	0.08	5.10	13.53	0.05	0.51
	0.15	20.30	0.15	20.35	0.08	0.25	19.03	0.13	-6.25
	0.2	26.89	0.15	26.39	0.07	-1.85	24.22	0.13	-9.93
	0.3	36.57	0.14	37.90	0.07	3.62	34.20	0.12	-6.50
	0.5	51.01	0.04	61.03	0.06	19.65	54.20	0.04	6.25
	0.7	69.05	0.10	82.84	0.05	19.98	73.44	0.09	6.36
	0.9	82.65	0.09	99.97	0.05	20.95	88.68	0.08	7.30
	1	81.64	0.04	93.18	0.05	14.14	81.24	0.03	-0.48
	1.2	105.01	0.08	121.79	0.04	15.98	108.47	0.07	3.30
	1.5	121.56	0.07	142.77	0.03	17.45	128.32	0.06	5.57
	2	141.21	0.05	169.48	0.03	20.02	153.95	0.05	9.02
	3	169.83	0.04	208.88	0.02	22.99	192.90	0.03	13.58
	4	184.08	0.04	228.06	0.02	23.89	212.47	0.03	15.42
	5	199.22	0.01	242.72	0.02	21.84	228.06	0.01	14.48
	7	217.71	0.03	263.61	0.02	21.08	250.25	0.03	14.95
	8	225.39	0.03	270.72	0.02	20.12	257.99	0.03	14.47
	9	226.24	0.03	270.19	0.02	19.42	257.76	0.03	13.93
	10	224.91	0.01	267.95	0.02	19.14	255.76	0.01	13.72
	12	227.77	0.04	270.80	0.02	18.89	259.32	0.03	13.85
	14	234.69	0.04	276.73	0.02	17.91	266.52	0.04	13.56
	15	236.20	0.02	278.95	0.02	18.10	268.86	0.01	13.82
	16	200.40	0.04	277.47	0.02	38.46	267.68	0.04	33.57
	18	204.50	0.05	280.50	0.03	37.16	271.59	0.04	32.81
	20	203.69	0.02	278.46	0.03	36.71	269.45	0.02	32.28

The error columns give the relative statistical error propagated from the uncertainty of the Monte Carlo simulations.
Relative difference denotes the percent difference of the effective dose coefficient ratio (bent/upright) from a ratio of 1.00.

List of Figures

Fig 13 Neutron and photon contributions to the absorbed dose coefficients for endosteum for selected energies in the AP irradiation geometry (upright male phantom).

Fig 14 Effective dose coefficient ratio in AP and PA irradiation geometries with PIMAL bent at 45° and 90° postures. A horizontal line for a ratio of 1.0 is provided as a visual reference for the reader.

Fig 15 Effective dose coefficient ratio in LLAT and RLAT irradiation geometries with PIMAL bent at 45° and 90° postures. A horizontal line for a ratio of 1.0 is provided as a visual reference for the reader.

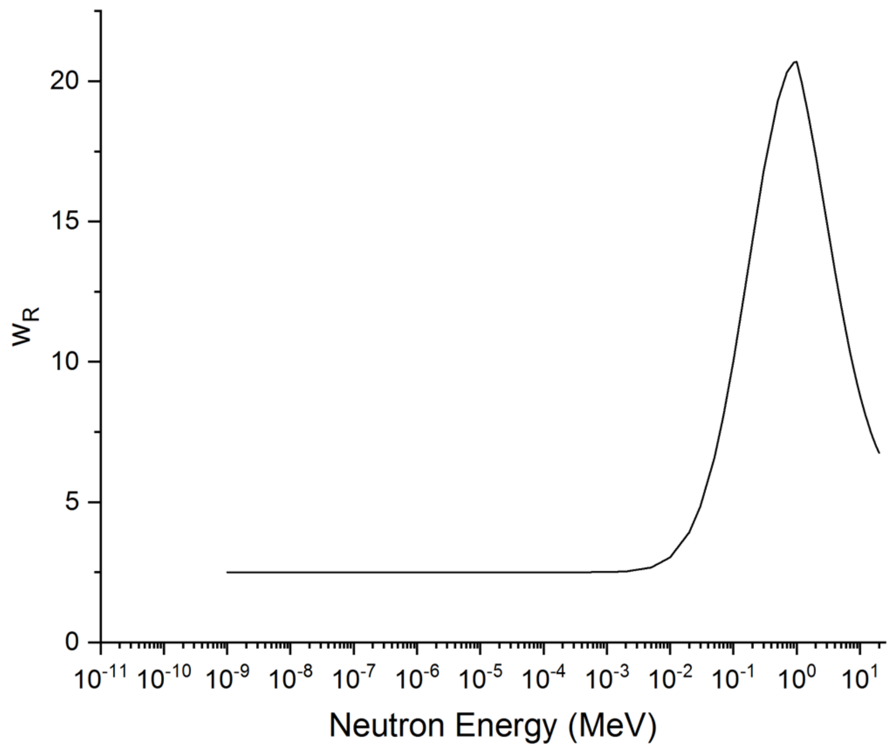

Fig 2 *Neutron weighting factor, w_R, as a function of neutron energy, shown for energies $1.0 \cdot 10^{-9}$ – 20 MeV.*

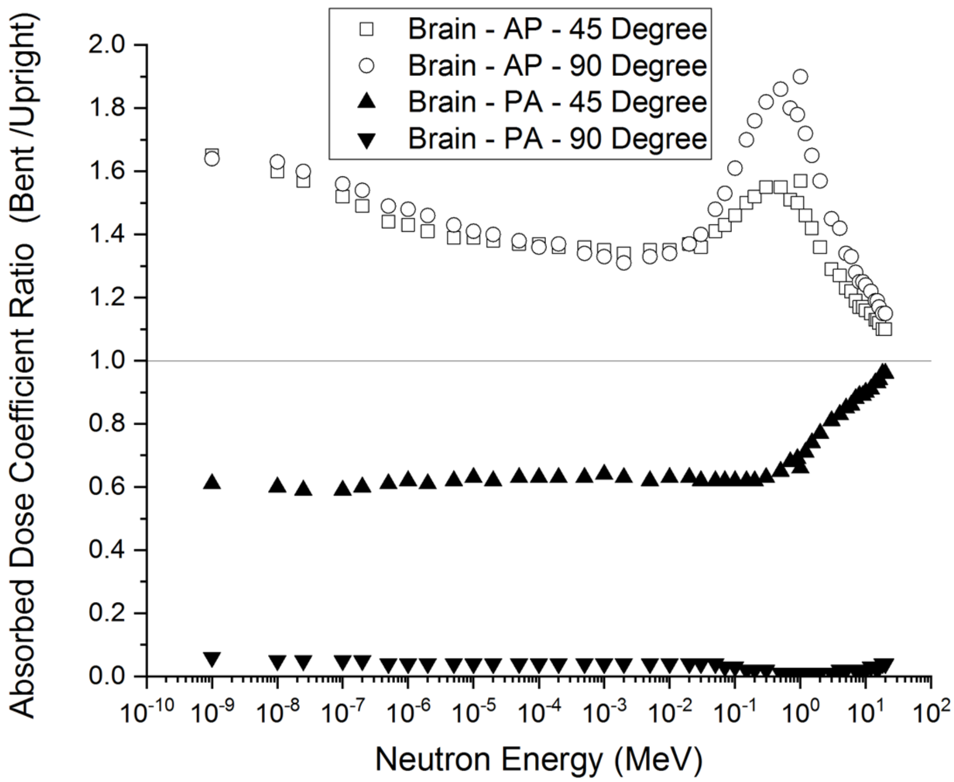

Fig 3 *Sex-averaged absorbed dose coefficient ratio for brain in AP and PA irradiation geometries with PIMAL bent at 45° and 90° postures. A horizontal line for a ratio of 1.0 is provided as a visual reference for the reader.*

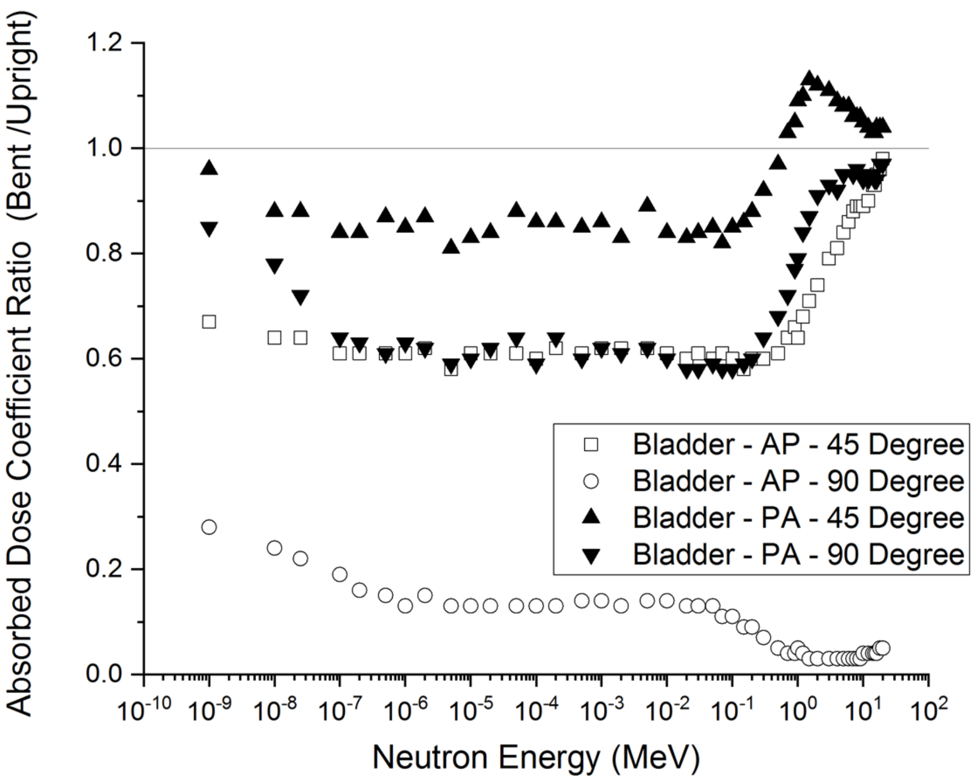

Fig 4 *Sex-averaged absorbed dose coefficient ratio for urinary bladder in AP and PA irradiation geometries with PIMAL bent at 45° and 90° postures. A horizontal line for a ratio of 1.0 is provided as a visual reference for the reader.*

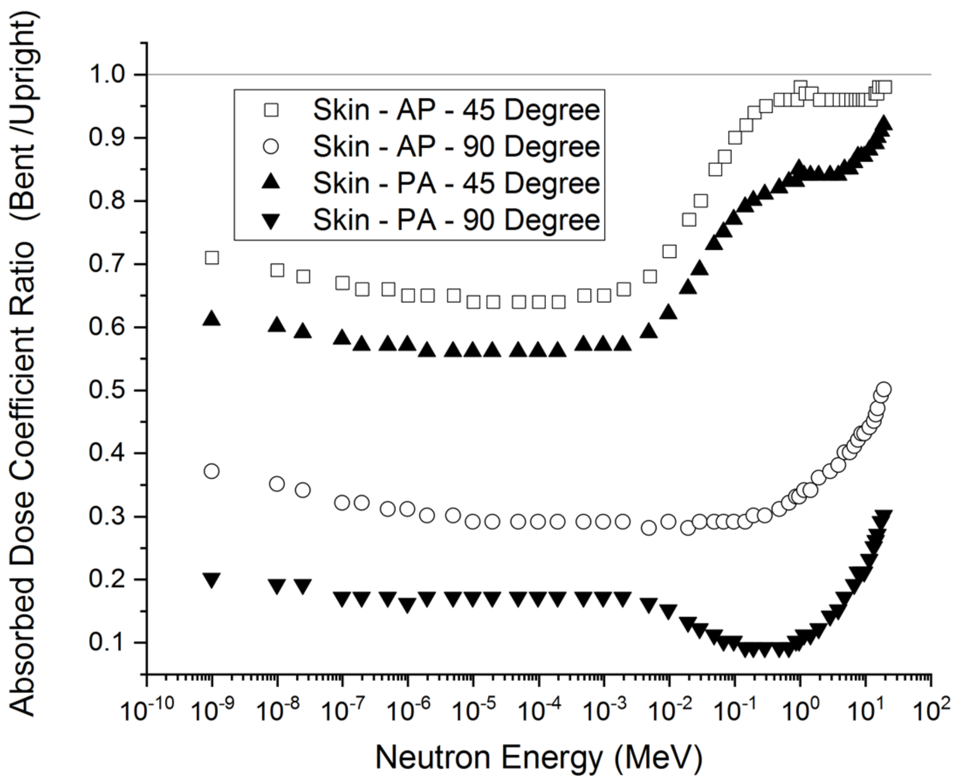

Fig 5 *Sex-averaged absorbed dose coefficient ratio for skin in AP and PA irradiation geometries with PIMAL bent at 45° and 90° postures. A horizontal line for a ratio of 1.0 is provided as a visual reference for the reader.*

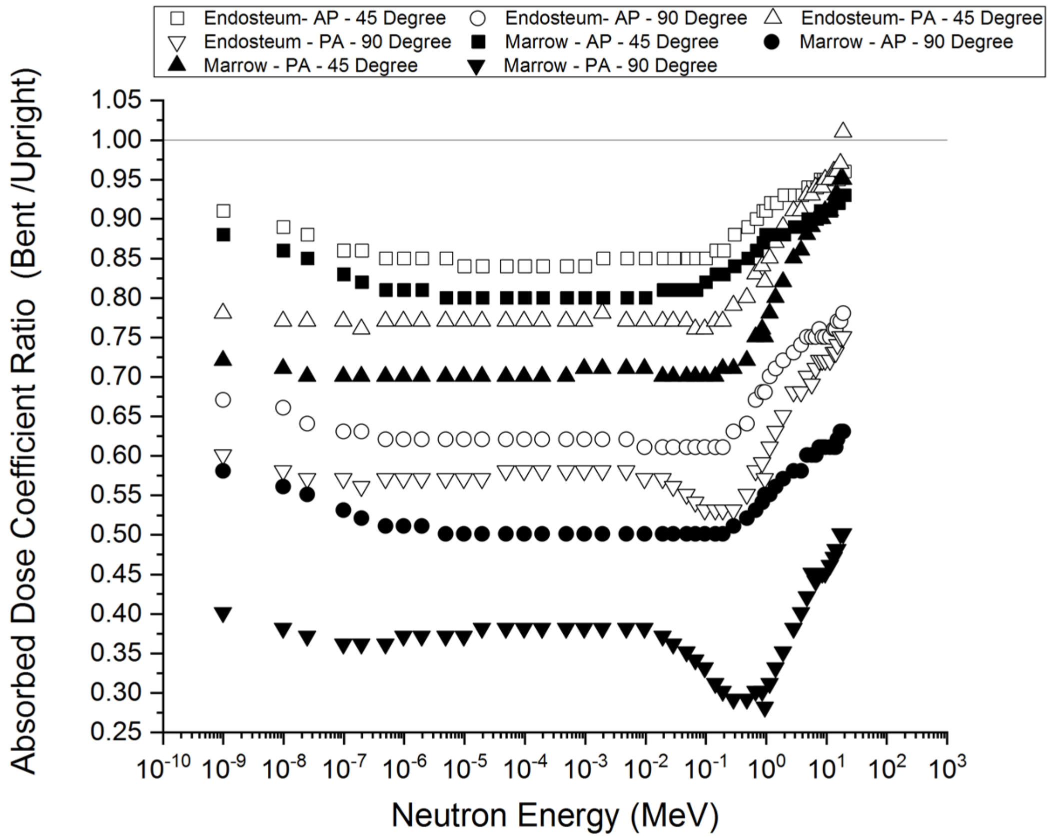

Fig 6 *Sex-averaged absorbed dose coefficient ratio for endosteum and active marrow in AP and PA irradiation geometries with PIMAL bent at 45° and 90° postures. A horizontal line for a ratio of 1.0 is provided as a visual reference for the reader.*

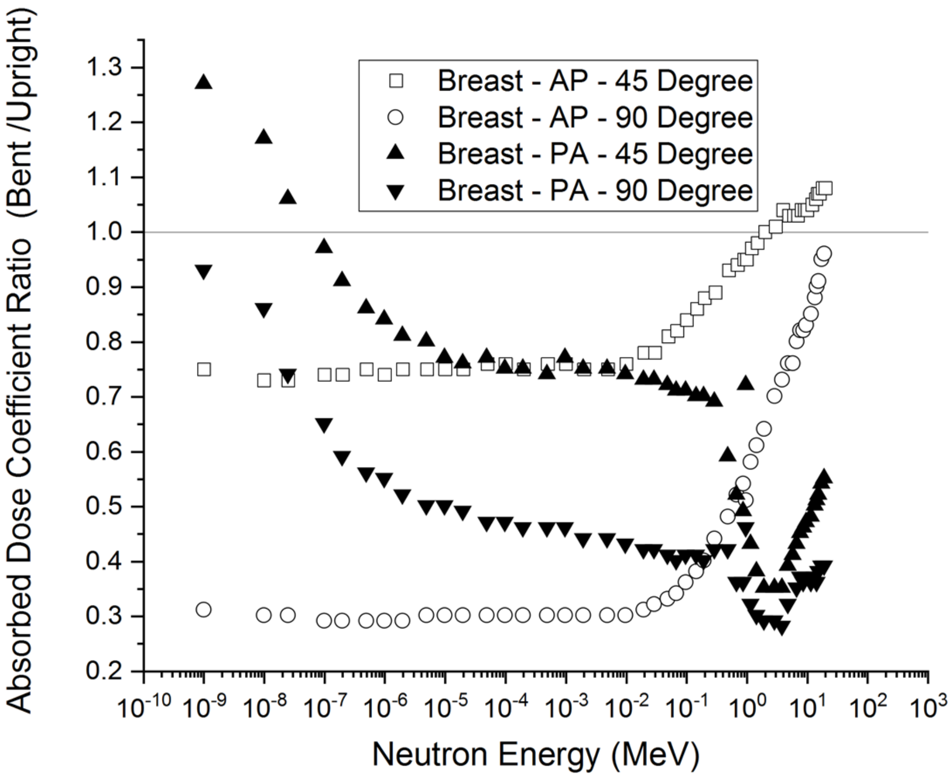

***Fig** 7 Sex-averaged absorbed dose coefficient ratio for breast in AP and PA irradiation geometries with PIMAL bent at 45° and 90° postures. A horizontal line for a ratio of 1.0 is provided as a visual reference for the reader.*

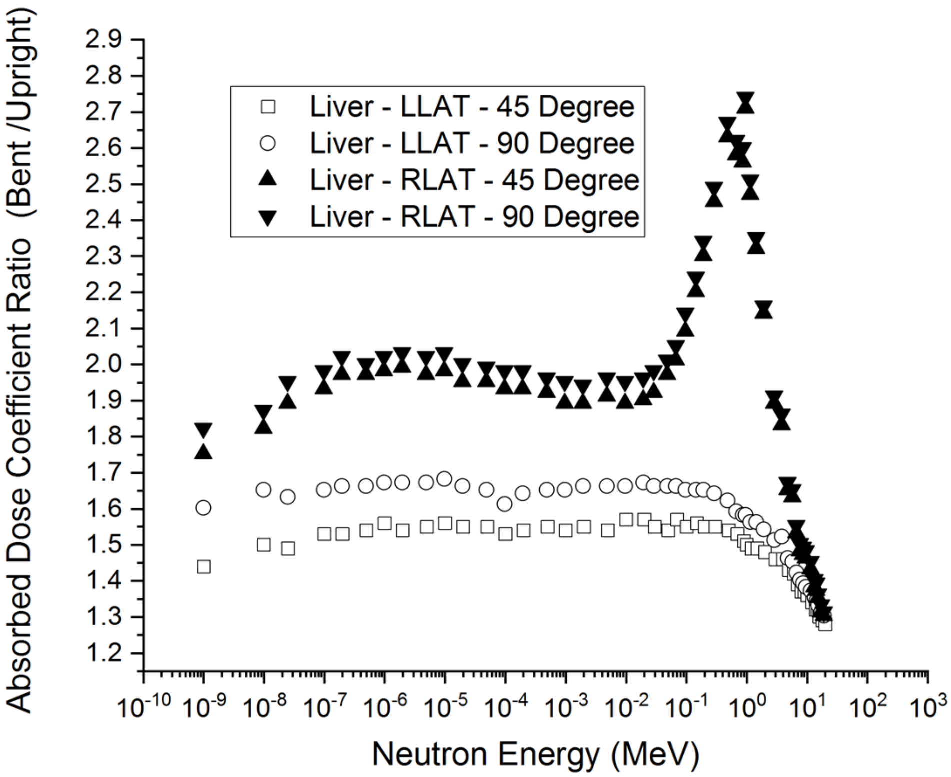

Fig 8 *Sex-averaged absorbed dose coefficient ratio for liver in LLAT and RLAT irradiation geometries with PIMAL bent at 45° and 90° postures.*

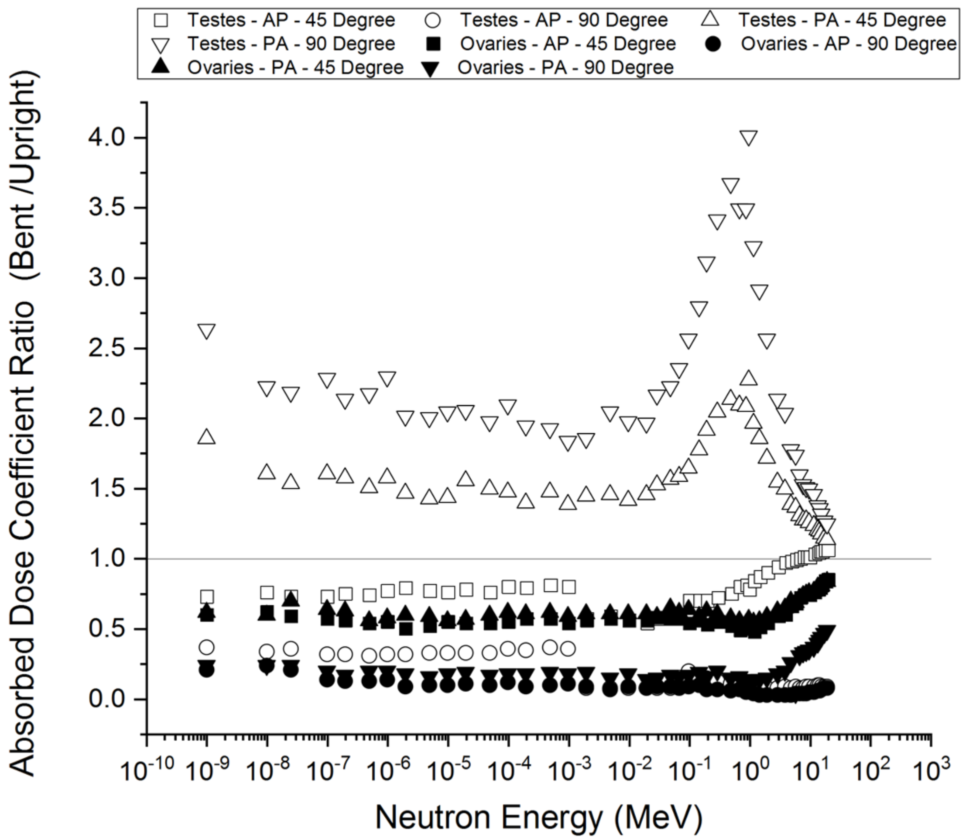

Fig 9 *Absorbed dose coefficient ratio for gonads (male: testes; female: ovaries) in AP and PA irradiation geometries with PIMAL bent at 45° and 90° postures. A horizontal line for a ratio of 1.0 is provided as a visual reference for the reader.*

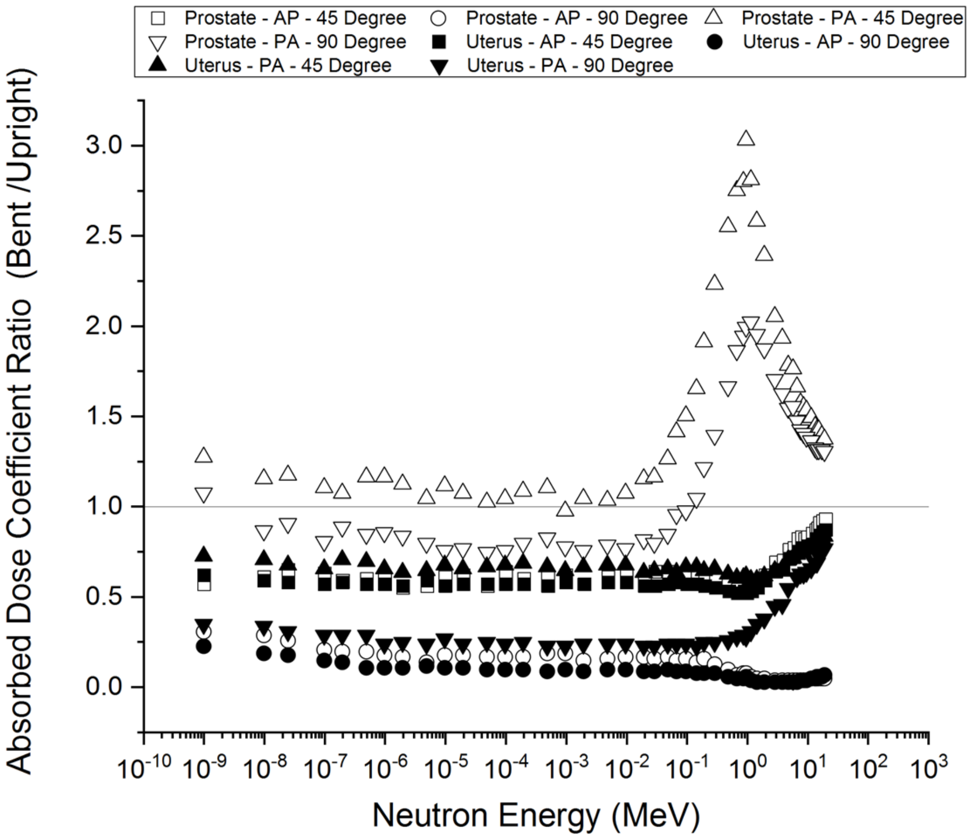

Fig 10 *Absorbed dose coefficient ratio for sex-specific organs (male: prostate; female: uterus) in AP and PA irradiation geometries with PIMAL bent at 45° and 90° postures. A horizontal line for a ratio of 1.0 is provided as a visual reference for the reader.*

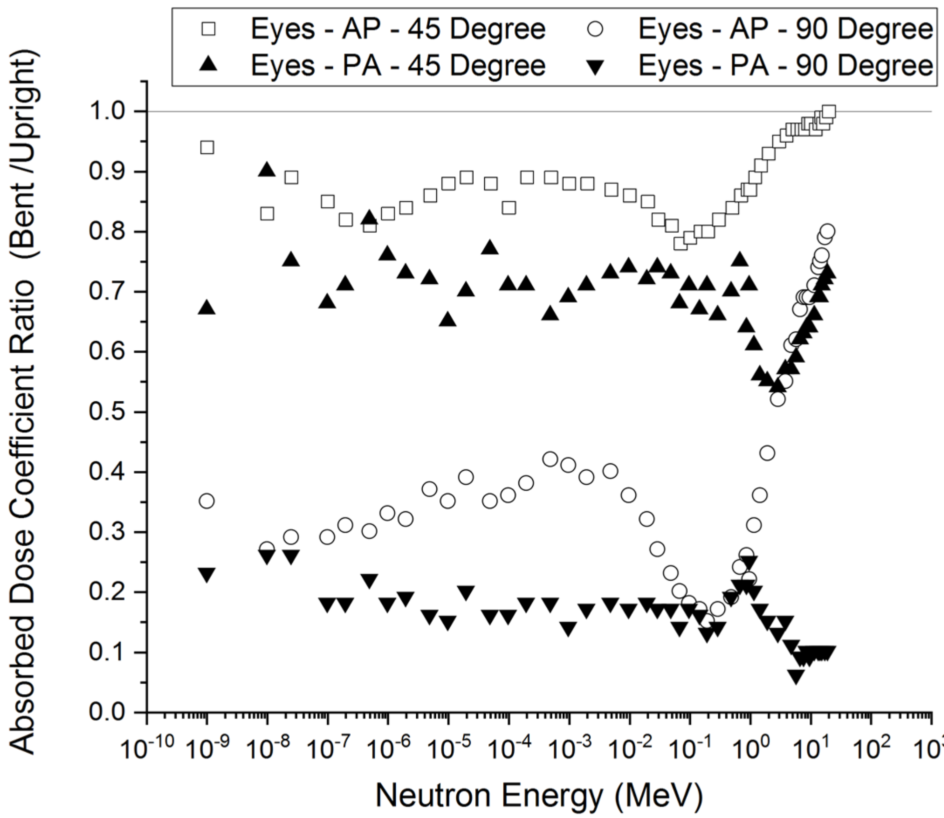

Fig 11 *Sex-averaged absorbed dose coefficient ratio for eyes in AP and PA irradiation geometries with PIMAL bent at 45° and 90° postures. A horizontal line for a ratio of 1.0 is provided as a visual reference for the reader.*

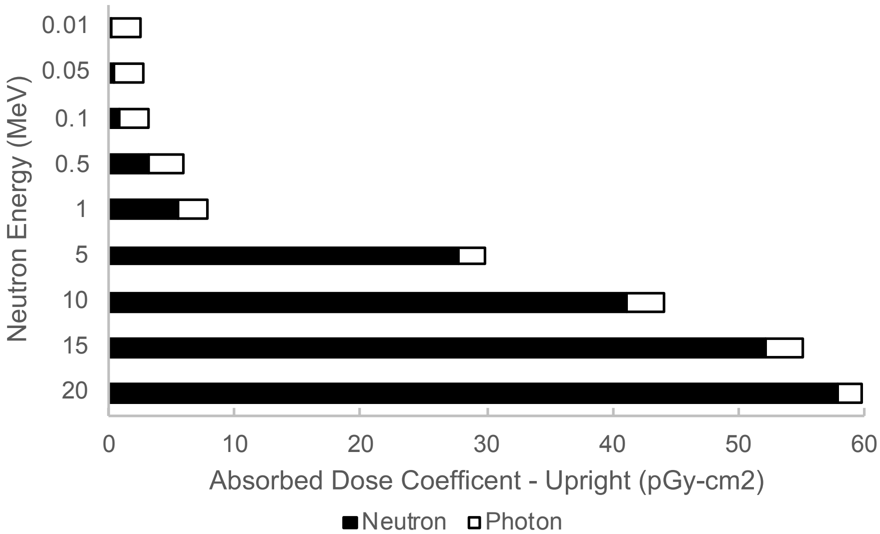

Fig 12 *Neutron and photon contributions to the absorbed dose coefficients for active marrow for selected energies in the AP irradiation geometry (upright male phantom).*

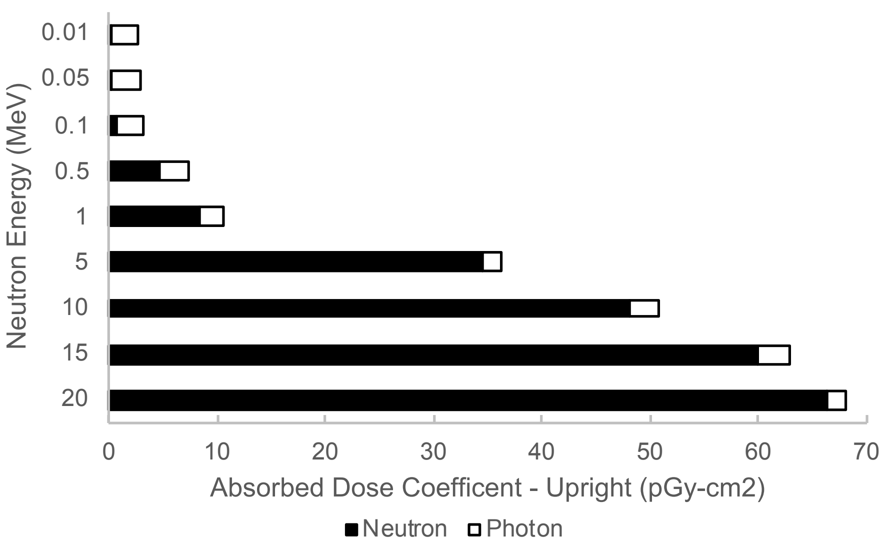

Fig 13 *Neutron and photon contributions to the absorbed dose coefficients for endosteum for selected energies in the AP irradiation geometry (upright male phantom).*

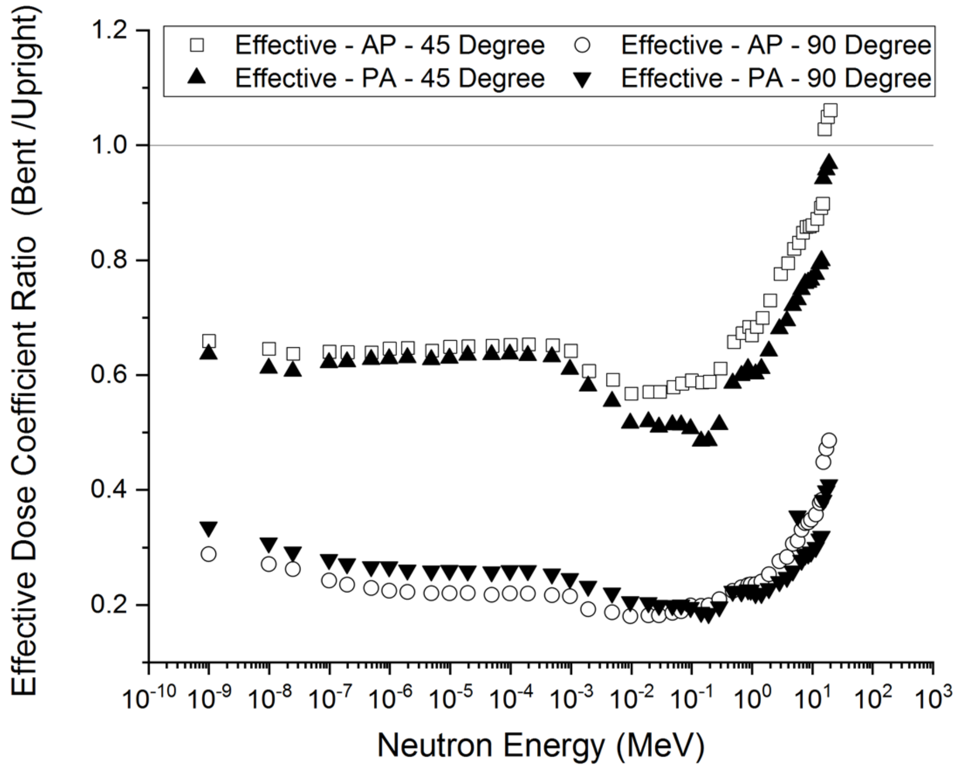

Fig 14 *Effective dose coefficient ratio in AP and PA irradiation geometries with PIMAL bent at 45° and 90° postures. A horizontal line for a ratio of 1.0 is provided as a visual reference for the reader.*

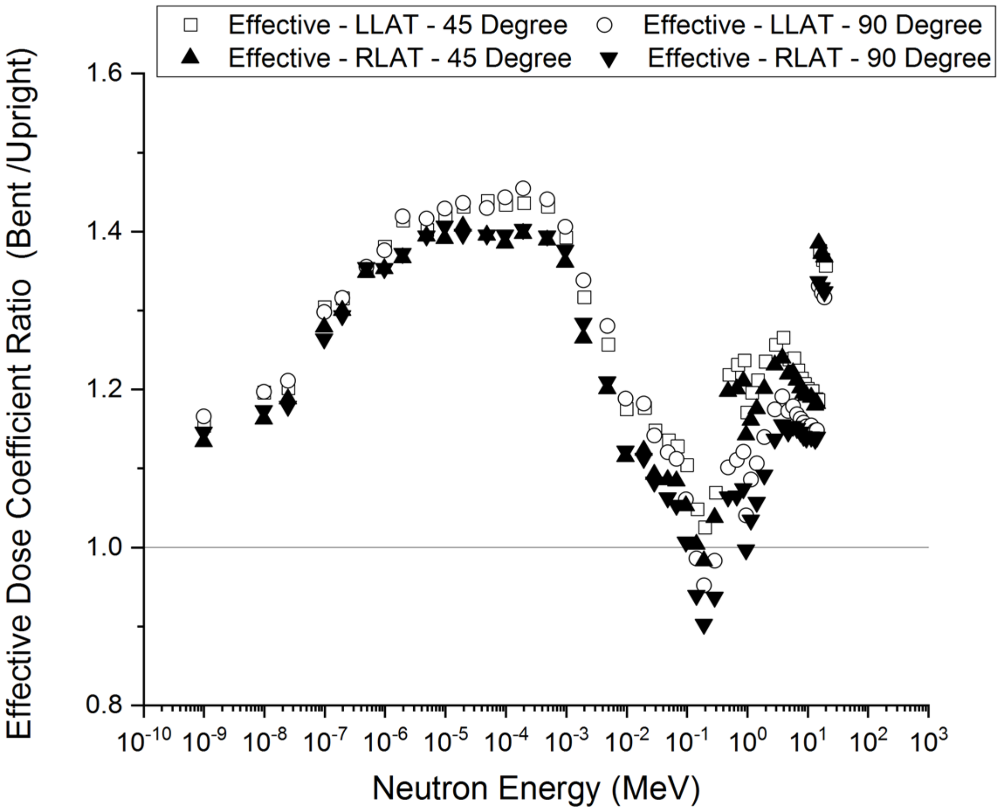

Fig 15 *Effective dose coefficient ratio in LLAT and RLAT irradiation geometries with PIMAL bent at 45° and 90° postures. A horizontal line for a ratio of 1.0 is provided as a visual reference for the reader.*

564